

# Using simplified linear and nonlinear models to assess ENSO-modulated MJO teleconnections

Marybeth C. Arcodia<sup>1,2</sup> · Ben P. Kirtman<sup>1</sup>

Received: 16 June 2022 / Accepted: 12 June 2023 © The Author(s), under exclusive licence to Springer-Verlag GmbH Germany, part of Springer Nature 2023

### **Abstract**

Simple dynamical models are used to understand fundamental processes of how ENSO modulates subseasonal teleconnections associated with tropical imprints of the MJO by stripping away complex phenomena. Both a dry linear baroclinic model and a dry nonlinear baroclinic model are employed to (1) assess how much of the MJO teleconnection pattern in a particular ENSO phase can be captured by linear and nonlinear dynamics and (2) analyze the role of the ENSO-modulated MJO forcing and base state in reproducing the teleconnection patterns. The modeling experiments reveal that linear dynamics are sufficient in capturing differences between the Northern Hemisphere teleconnections associated with the MJO during El Niño and La Niña. Nonlinear dynamics modestly capture more of the Northern Hemisphere MJO teleconnection pattern, particularly over North America, suggesting the teleconnection response over North America is more complex. The teleconnection patterns are sensitive to changes in both the ENSO background state and the domain of the monthly MJO-associated forcing. A Rossby wave source diagnosis is applied to further understand the underlying mechanisms. Further, a series of experiments swapping MJO forcings during El Niño events versus La Niña events with an ENSO-neutral base state and vice versa show that the MJO forcing has a larger influence over the teleconnection pattern than the base state. Therefore, the modulation of the MJO convection by ENSO dominates the ENSO-phase-dependent changes to the Northern Hemisphere teleconnection pattern. These modeling experiments highlight that MJO teleconnections must be considered in the context of the ongoing ENSO event.

### 1 Introduction

The MJO produces robust and consequential teleconnection patterns in the Northern Hemisphere via upper-level divergent flow associated with the MJO convective disturbance forcing Rossby wave trains emanating from the tropics to the extratropics (Riehl 1950; Hoskins and Karoly 1981). These MJO teleconnections in the Northern Hemisphere during boreal winter have been found to affect temperature (Seo et al. 2016), circulation (Henderson et al. 2016), and precipitation patterns (Becker et al. 2011; Arcodia et al. 2020) via interaction with the Asian-Pacific jet (Kim et al. 2006), the Pacific-North American pattern (Mori and Watanabe 2008; Riddle et al. 2013), and the North Atlantic Oscillation

(Cassou 2008). While the MJO is the dominant mode of subseasonal variability in the tropics, ENSO is the dominant mode of interannual variability in the tropical Indo-Pacific and it is a spatially stationary phenomenon, at least on the timescales of the MJO. In a similar way to the MJO, ENSO has its own teleconnections and the effects on atmospheric circulation patterns, temperature, and precipitation have been documented throughout the globe (Alexander et al. 2002; Diaz et al. 2001; Yeh et al. 2018).

According to Matthews et al. (2004), the effect of the basic states of El Niño and La Niña is of the same qualitative importance as the effect of the nonlinear response within the standard MJO cycle. ENSO modulates the background state through which the MJO is propagating, and has been shown to modulate the MJO strength, propagation speed, and pattern evolution (Pohl and Matthews 2007; Wei and Ren 2019; Yadav and Straus 2017; Liu et al. 2020; Wang et al. 2018; Hsu et al. 2018). Teleconnection patterns are dependent on the mean state of both the atmosphere and the ocean, and modulation of the mean state can affect the persistence, location, and strength of the extratropical teleconnection

Published online: 22 June 2023



Marybeth C. Arcodia marcodia@rsmas.miami.edu

Rosenstiel School of Marine, Atmospheric, and Earth Science, University of Miami, Coral Gables, USA

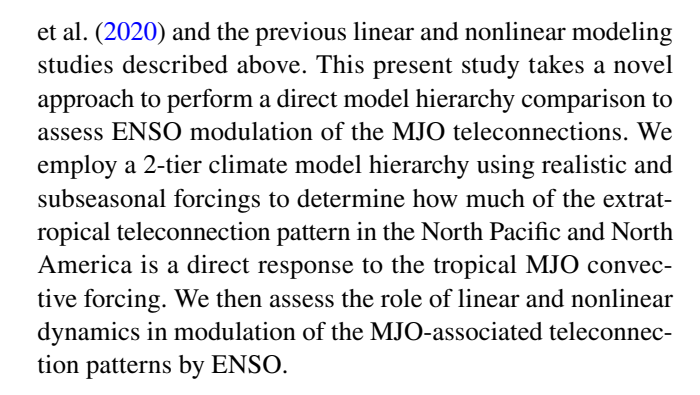
<sup>&</sup>lt;sup>2</sup> Colorado State University, CO, Fort Collins, USA

in response to the tropical disturbance (Ting and Sardeshmukh 1993; Stan et al. 2017; Yeh et al. 2018; Henderson and Maloney 2018; Wang et al. 2020b). A number of studies have assessed how ENSO modulates MJO teleconnections, resulting in changes to teleconnection patterns in the Northern Hemisphere (Moon et al. 2011; Hoell et al. 2014; Lee et al. 2019). The study of Arcodia et al. (2020) analyzes how the specific location of the deep convection associated with the MJO, combined with the modulation of the background state by ENSO, affects the rainfall teleconnection signal in the U.S. via constructive and destructive interference. Lower frequency phenomena have also been found to affect the MJO and its associated teleconnection patterns such as the Quasi-Biennial Oscillation (QBO; Mayer and Barnes 2020; Feng and Lin 2019; Son et al. 2017).

Separating the linear and nonlinear influences is challenging since the interaction between the MJO and ENSO is at least partly nonlinear, although it does not imply that the remote responses are nonlinear (Feng et al. 2015; Pang et al. 2016). Roundy et al. (2010) emphasizes that nonlinearity in the climate system negates the ability to composite MJO and ENSO teleconnection patterns separately. While Roundy et al. (2010) find that simply linearly combining the responses from MJO and ENSO is insufficient, Riddle et al. (2013) note that some occurrences of certain weather regimes are due to nonlinear contributions of MJO and ENSO, while other occurrences are due to linear combinations.

Due to the complexities of linear and nonlinear impacts from ENSO on MJO teleconnections, modeling the teleconnections associated with the MJO offers more insights into ENSO's impact via modulation of the mean state and the MJO itself. For MJO teleconnections to be represented well in models, both the mean state (Dawson et al. 2011; Weare 2013; Ling et al. 2019) and the MJO itself need to be well represented (Henderson et al. 2017; Yoo and Son 2016; Wang et al. 2020a), but this remains a difficult task. Thus, simple models are employed in this study in which the forcing and the mean state are explicitly prescribed to directly analyze the role of each. Using a linear baroclinic model, Tseng et al. (2019) reasonably reproduced the MJO-induced teleconnections observed in the reanalysis data, and found that MJO phases 2–7 generate consistent teleconnection patterns in the Pacific-North American region with higher 2-4 weeks lead time forecast skill. Tseng et al. (2020) further analyzed the joint influence of the basic state and MJO forcing on the teleconnection pattern, finding that MJOs during El Niño years offer less subseasonal predictability. Using a nonlinear baroclinic model, Henderson and Maloney (2018) found that the background ENSO state affects the role of the MJO on high-latitude blocking events.

This study expands upon the ENSO-modulated teleconnection patterns documented from reanalysis in Arcodia



### 2 Model setups, data, and methods

We use a linear and nonlinear framework via a 2-tier climate model hierarchy to assess which aspects of the background state and forcing during an MJO and ENSO phase combination during boreal winter months are important in producing the Northern Hemisphere teleconnection response.

A dry linear baroclinic model (LBM; Watanabe and Kimoto 2000) is employed to document how much of the subseasonal teleconnections associated with the MJO in the Northern Hemisphere midlatitudes can be captured by strictly linear dry dynamics to investigate the responses during different ENSO base states and later compare nonlinear dynamics results. The use of a simple linear model is motivated by the ability to investigate complex atmospheric phenomena in a simple way by stripping the complicated nonlinear mechanisms from the system. In a linearized model, it is possible to separate the anomalous response from the basic state, which would not be possible in a model with feedback processes (Tseng et al. 2019). The LBM version used in this study has been used to successfully diagnose tropical-extratropical teleconnection mechanisms on subseasonal timescales, such as the MJO influencing U.S. tornado genesis (Kim et al. 2020) and the East Asian Monsoon influencing U.S. heatwaves (Lopez et al. 2019). Tseng et al. (2020) also used an ensemble version of the LBM to assess interannual variability of MJO teleconnection consistency between MJO phases. The model includes no radiative feedbacks, convection, or moisture, so the complications of parameterization with convective schemes and precipitation are eliminated. Deep convection is instead represented with prescribed diabatic heating associated with convection. A model without moisture or tropical convection can still produce subseasonal variability and a Kelvin-wave structure resembling the MJO (Lin et al. 2007).

Since the midlatitude response can be greatly influenced by extracting energy from the mean flow (Simmons et al. 1983), the role of large-scale atmospheric instabilities and nonlinear feedbacks should also be considered when exploring the mechanism of MJO teleconnection patterns and



their modulation by ENSO. In the second tier of the climate model hierarchy, we employ a dry nonlinear atmospheric general circulation model (AGCM; Kirtman et al. 2001) to assess the limitations of the simple linear interpretation of the tropical–extratropical teleconnections from the LBM.

AGCMs or similar models have proven useful for exploring variability in teleconnection responses to diabatic heating forcing (Straus and Shukla 2000; Higgins and Schubert 1996; Straus et al. 2015; Seo and Lee 2017). Kirtman et al. (2001) used a version of the AGCM used in this study and found that variations in subseasonal SST anomalies produced significant variations in North American rainfall and 500 mb geopotential height patterns. Recently, Malloy and Kirtman (2022) used the AGCM to study East Asian Monsoon teleconnections and found that the model captured the primary dynamical processes of the North American Subtropical High and some processes that affect the North American Low-Level Jet.

### 2.1 Linear baroclinic model (LBM)

### 2.1.1 LBM setup

The dry linear baroclinic model (LBM; Watanabe and Kimoto 2000) is used to diagnose the direct teleconnection response from an imposed forcing associated with the MJO. The LBM is a primitive equation model linearized around a base state. The model is run at a horizontal resolution of T21 (roughly 5.5° latitude) with 11 vertical levels (T21L11). Eleven vertical levels allows for enough resolution of the vertical structure of the basic state winds, including the jet core tilting poleward with height, which is important for Rossby wave forcing through differential vorticity advection (Lopez et al. 2019). This study is concerned primarily with the spatial structure of the MJO teleconnections, which can be captured with T21 as shown in Kim et al. (2020). The steady-state solution using the full matrix inversion technique (Hoskins and Karoly 1981; Watanabe and Kimoto 2000) is used, allowing for wave-wave interactions with truncation at zonal wavenumber 15. Drag is applied to the model in the form of Rayleigh friction and Newtonian cooling, with a timescale of 0.25 day<sup>-1</sup> at the low levels, 0.5 day<sup>-1</sup> at the upper levels, and 10 day<sup>-1</sup> in the middle levels, as these values produced the most reasonable results without nearly resonant responses from too little damping. These parameters are the same for all experiments, so that the differences in the LBM results are due to only differences in imposed forcing and the basic state.

### 2.1.2 LBM forcing

To model the tropical convection, we impose diabatic heating into the model since there are no moisture terms. To

prescribe the horizontal structure of the heating, we use the rainfall from NCEP-NCAR Reanalysis-2 (Kalnay et al. 1996) following the methodology described in Arcodia et al. (2020), which justified the use of NCEP reanalysis precipitation for identifying potential drivers of spatial variation in the rainfall anomalies. The Tropical Rainfall Measuring Mission (TRMM; Simpson et al. 1996) dataset (a shorter, e.g. 1998-2017, but higher resolution observational precipitation dataset) was also used to test the sensitivity of the results to the rainfall dataset used to calculate the diabatic heating, but the extratropical response remained similar with the same general large scale structures persisting in the North Pacific and North America. The precipitation anomaly used here is the daily anomaly (daily climatology subtracted) minus the 120-day centered running mean, where the 120day centered running mean effectively captures the variability associated with ENSO (Lin et al. 2008; Arcodia et al. 2020). Only November–April months are used as the boreal winter is the active season of the MJO (Zhang 2005). The anomalous rainfall associated with the tropical MJO forcing is converted into diabatic heating using the following equation derived from the moisture equation:

$$\dot{Q}'(x,y,t,p) = \left(\frac{L_{\nu}\rho g}{c_{\nu}p_{s}}\right) \left(precip'(x,y,t)\right) \left(\eta(p)\right) \tag{1}$$

where  $\dot{Q}'$  is the diabatic heating anomaly,  $L_{\nu}$  is the latent heat of vaporization,  $\rho$  is the density of air, g is gravity,  $c_p$  is the specific heat of water,  $p_s$  is the surface pressure, and  $\eta(p)$  is the normalized vertical structure such that

$$\int_0^{p_s} \eta(p)dp = 1 \tag{2}$$

and the precipitation anomaly is that associated with the MJO tropical forcing. A full derivation of the anomalous diabatic heating is in the "Appendix". The 2-dimensional diabatic heating field is then multiplied to a specified vertical structure profile to create a 3-dimensional anomalous diabatic heating forcing (more detail in the *Vertical Profile Sensitivity Testing* section). Previous studies have used a similar approach in forcing the LBM with a vertical heating profile particularly for the inverse matrix solver version of the model used here (e.g. Lopez et al. 2016; Kim et al. 2020.

The prescribed forcings are constructed with three simultaneous constraints: month, MJO phase, and ENSO phase. First, months are considered separately, as Newman and Sardeshmukh (1998) show the importance of month-tomonth variability is lost when averaging over 4–6 months. Additionally, Roundy et al. (2010) show that linear summation of MJO teleconnection patterns and ENSO teleconnection patterns is insufficient in capturing the correct response, so composites must be calculated based on concurrent MJO and ENSO phase. The MJO phase is diagnosed using the



Real-time Multivariate MJO Index outlined in Wheeler and Hendon (2004). MJO Phases 2 & 3, 4 & 5, 6 & 7, 8 & 1 (hereafter P23, P45, P67, P81) are combined to increase sample size and only those days with an RMM≥1.0 (active MJO) are considered. ENSO phases are separated into three categories: warm ENSO (El Niño events), cold ENSO (La Niña events), and neutral events. El Niño (warm) and La Niña (cold) ENSO periods are defined by the NOAA Climate Prediction Center (CPC): exceeding a threshold of  $\pm 0.5$  °C for the oceanic Niño index (ONI), a 3-month running mean of ERSST.v5 SST anomalies in the Niño-3.4 region (5°N-5°S, 120°-170°W), based on centered 30-yr base periods updated every 5 years. Neutral periods fall within the threshold. Put simply, for each experiment, the monthly mean forcings are constrained by simultaneous MJO phase and ENSO phase. For example, the daily rainfall anomaly for all the days in November from 1979 to 2017 in which the MJO was active and is P23 and an El Niño was present would be used to calculate the diabatic heating following Eq 1., then averaged to create one forcing for an LBM run. A separate run uses the daily anomalies composited from all the December days in which the MJO was active and in P23 and El Niño was present, and so on. The same process for creating the forcings is done for La Niña days and ENSO Neutral days. The averaged response is then calculated using a weighted average for the number of days used for each forcing to average over the November-April period while still retaining the monthly variability. A table with the number of each days for each monthly, MJO, and ENSO constraint can be found in Table 1. For comparison of the LBM output to reanalysis and the AGCM output, 500 mb geopotential height is used for assessing the teleconnection response patterns. The 500 mb geopotential height output in the LBM is the direct response to the anomalous forcing and the zonal mean is removed to isolate the anomalous response. The same process was applied to the comparisons with the nonlinear AGCM and the reanalysis data.

### 2.1.3 LBM base state

The base states for the following experiments are zonally asymmetric 3-D fields constructed from NCEP-NCAR Reanalysis-2 daily data from 1979 to 2017 to be consistent with Arcodia et al. (2020), as this study serves as the primary motivation for this study. As with the forcings, only November-April months are used as the boreal winter is the active season of the MJO (Zhang 2005). However, the base states are only constrained by ENSO phase, not individual months or MJO phase as in the forcings, to ensure to ensure that the background flow does not include the expected anomalous model response to the forcing, and thus the response to MJO forcing is an anomaly relative to the basic state. Thus, an El Niño NDJFMA base state, a La Niña NDJFMA base state, and an ENSO Neutral NDJFMA base state are constructed.

## 2.2 Dry atmospheric general circulation model (AGCM)

### 2.2.1 Dry AGCM setup

The second climate model used in this study is a dry baroclinic nonlinear atmospheric general circulation model (AGCM). It is a primitive equation spectral model with Rhomboidal truncation at R15 which equates to roughly 4.5° latitude by 7.5° longitude with 11 vertical sigma levels. These resolutions were chosen to best match with the LBM model resolutions. The model has been adapted by Kirtman et al. (2001) from Brenner et al. (1984) and has removed all moisture components and processes. Newtonian cooling and Rayleigh friction are applied; realistic topography is used and provides a topographical forcing. The model is described in further detail in Brenner et al. (1984) and Malloy and Kirtman (2022) and versions of this model have been employed in Kirtman et al. (2001) and Malloy and Kirtman (2022).

Table 1 The number of days for each simultaneous monthly, MJO, and ENSO constraint used for the LBM and AGCM experiments

El Niño days				La Niña days				Neutral days						
Month	MJO phase				Month	MJO phase				Month	MJO phase			
	P23	P45	P67	P81		P23	P45	P67	P81		P23	P45	P67	P81
November	125	46	38	74	November	40	73	103	44	November	34	43	69	51
December	91	63	61	43	December	38	51	65	41	December	72	43	63	56
January	50	54	88	37	January	109	55	68	70	January	85	49	71	56
February	40	33	61	58	February	76	57	53	43	February	54	58	81	60
March	74	79	69	86	March	66	56	51	44	March	77	67	87	86
April	53	36	41	44	April	53	60	62	42	April	81	77	75	88



### 2.2.2 Dry AGCM forcing and base state

The forcings and base states used in the AGCM follow the same procedure as in the LBM. For every run, the model is run for 1200 days with the first 100 days discarded to account for spin-up, resulting in a 1100-day run per experiment. Each run of the AGCM utilizes an ENSO-phase dependent base state (i.e. the temperature field used in the Newtonian cooling) and a forcing composited in the same way as the LBM using the three conditions specified above: month, MJO phase and ENSO phase.

A control run is completed for each base state in which the AGCM is run fully with no external forcing (i.e. no diabatic heating) and the only forcing in the model is internal (i.e. topographic). To assess the teleconnection response in the model to the imposed forcing, we take the response from the AGCM run forced with the diabatic heating and subtract the response from the unforced control run. This process is repeated for each AGCM run with a different forcing based on month, MJO phase and ENSO phase. For example, the AGCM is run with an ENSO-dependent climatological base state and MJO-associated diabatic heating forcing calculated by averaging over all days in November from 1979 to 2017 in which the MJO was active and in P23 and an El Niño was occurring. The model is re-run for the same climatological base state, but with no imposed diabatic heating, as a control run. The geopotential height is calculated for each output following Malloy and Kirtman (2022) and this response is subtracted from the response from the forced run. The time mean is taken over the 1100-day output and then the zonal mean is subtracted to find the anomalous eddy response to the forcing. The AGCM output for each month is weighted by the number of days used in the forcing for that month and a weighted average is calculated for MJO P23, P45, P67, and P81 with El Niño days, La Niña, Neutral days separated, respectively.

### 3 LBM experiments

A number of sensitivity tests were run with the LBM to confirm that the teleconnection response assessed was that due to the linear dynamics associated with the imposed forcing, and not an artifact of the model.

### 3.1 Vertical profile sensitivity testing

Vertical and horizontal representation of the structure of the heating is necessary for diagnosing how convection associated with the MJO, for example, affects circulation (Schumacher et al. 2004; Zhang and Mu 2005; Lappen and Schumacher 2012). In this study, the horizontal structure of the diabatic heating is directly specified by the

2-dimensional anomalous precipitation pattern taken from reanalysis, and thus is accurately represented to the extent that reanalysis rainfall captures the observed phenomenon. A vertical structure must then be specified to create a 3-dimensional diabatic heating profile to force the model. It is known that in the tropics, top-heavy diabatic heating profiles occur most frequently, but some bottom-heavy vertical profiles can be necessary for MJO convective organization and propagation (Lau and Peng 1987; Schumacher et al. 2004; Benedict et al. 2013; Stephens et al. 2019).

We test the sensitivity of the model response to four vertical profiles (shown in Fig. 1) in both the MJO Domain (top) and the Full Globe (bottom). The vertical profiles tested included "Realistic" (Fig. 1ai; i.e. top-heavy), "Low-level Heating" [Fig. 1a(ii); i.e. bottom-heavy], "Low-level Cooling" [Fig. 1a(iii)], and "Vertically Uniform" [Fig. 1a(iv)]. These sensitivity tests show that although there are small changes in magnitude, the spatial pattern of the teleconnection response to the MJO is not highly sensitive to the vertical profile. This is likely due to a lack of moisture-convective feedbacks in the model and the steady-state solution version of the model used, in which a time-varying and propagating MJO forcing is not being simulated, but rather imposed. The teleconnection response may become more dependent on the spatially-varying structure of the vertical profile in a higher vertical resolution of this model, but that is beyond the scope of this study. We find that the teleconnection patterns are much more dependent on the domain of the forcing than the vertical profile, so attention for subsequent experiments is focused on changes to the forcing domain and base state due to the ENSO background state.

The realistic vertical profile used for all subsequent experiments [see Fig. 1a(i)] is adapted from Lin et al. (2004) and has the maximum heating from 300 to 500 mb replicating mid-level condensational heating due to convection, with no heating at the topmost and bottom most layers. Additionally, since the model response is fairly insensitive to changes in the vertical profile, the same profile is used for all MJO forcings regardless of ENSO background state. While accurate vertical profile representation is fundamental for accurate MJO characterization, this study directly imposes the MJO forcing via diabatic heating and is not concerned with simulating MJO initiation or propagation, further justifying the use of the same vertical profile throughout the globe.

### 3.2 Forcing domain sensitivity testing

A series of experiments were also conducted to test how the forcing domain influences the teleconnection response. Figure 2 shows the forcing composited by month for each MJO phase during La Niña days, then averaged weighted by days per month for P23, P45, P67, and P81. The *MJO Domain* (Fig. 2a) run isolates the region with the largest



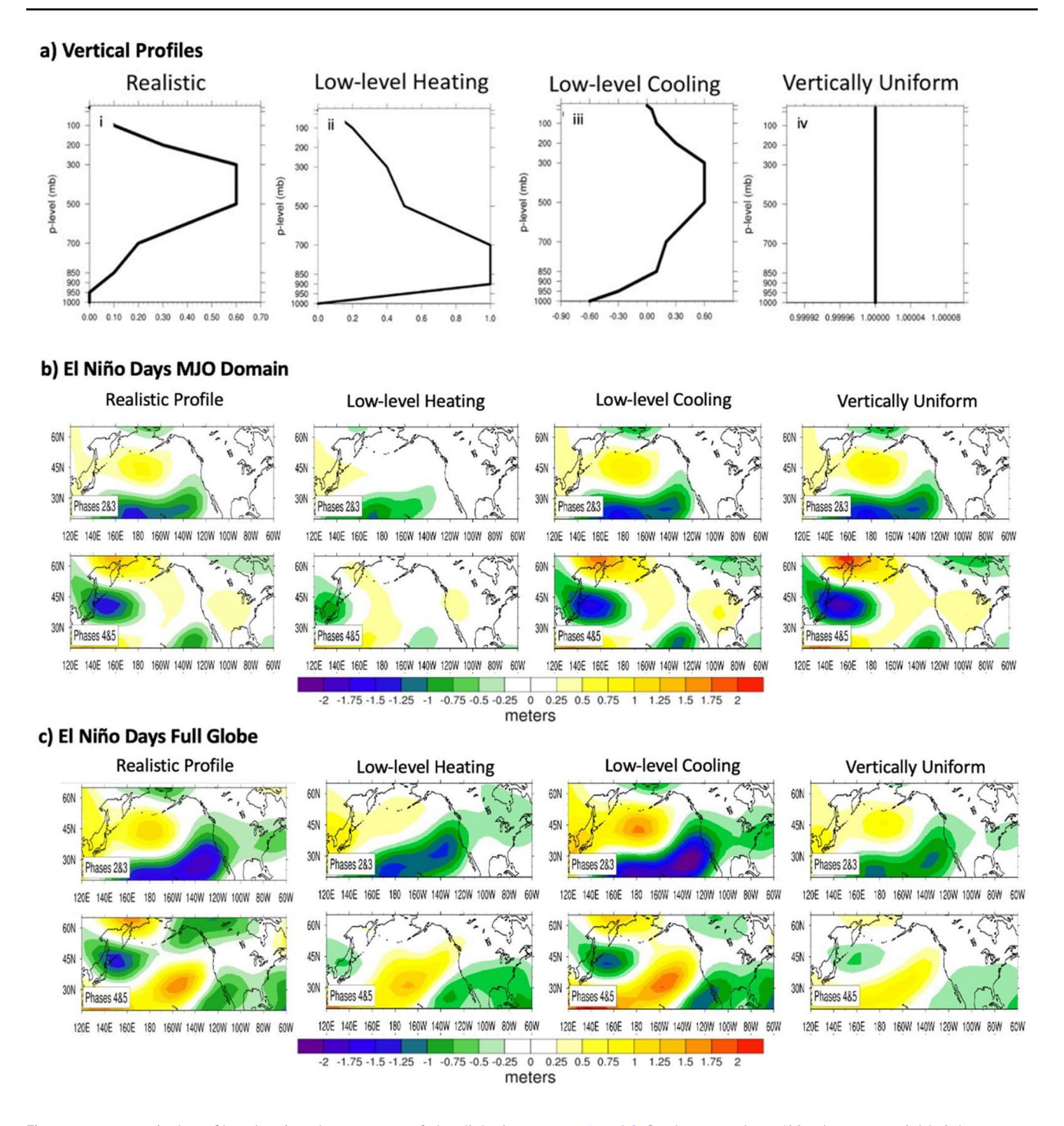


**Fig. 1** a Four vertical profiles showing the structure of the diabatic heating for the forcing in the LBM: (i) "Realistic"-maximum heating from 300 to 500 mb; (ii) "Low-level Heating"-maximum heating from 700 to 850 mb; (iii) "Low-level Cooling"-negative heating (cooling) below 900 mb; (iv) "Vertically Uniform"-equal heating applied throughout the column. The x-axis is non-dimensional and normalized to be applied to the diabatic heating profiles following

Eqs. 1 and 2. **b** The anomalous 500 mb geopotential height response from the LBM for the MJO domain forcing using the four vertical profiles in **a** during El Niño days for MJO P23 and P45. Each panel consists of the weighted average of the monthly response from November to April. **c** Same as **b** but for the Full Globe forcing domain

MJO-associated anomalies (25 S–25N, 40E–240E) to test if the forcing in the tropical Indo-Pacific diabatic heating dominates the extratropical teleconnection response. The *North* 

*Pacific Only* (Fig. 2b) run isolates the Northern Hemisphere extratropical region of 25N–45N to test the role of the leading North Pacific anomaly on the North American response.



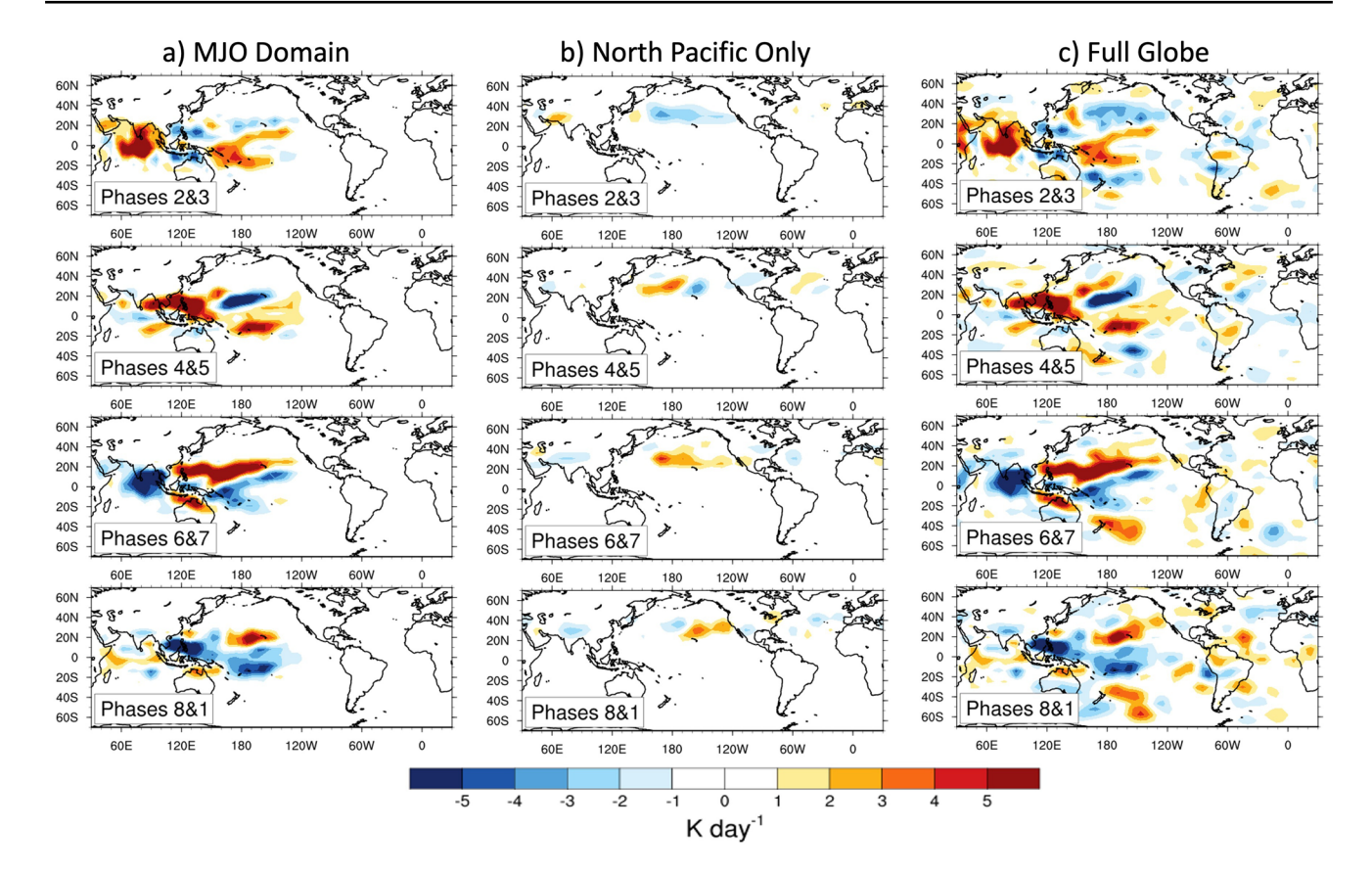


**Fig. 2** The anomalous 700 mb diabatic heating forcing domains for the MJO-forced experiments for La Niña days. Each panel consists of a weighted average of the number of days from each month November-April for the corresponding MJO phase and a La Niña was occur-

ring. **a** MJO-Domain Experiment: 25 S–25N; 40E–240E. **b** North Pacific Only Experiment: 25N–45N. **c** Full Globe Experiment: no domain restrictions. All forcings are in units of K day<sup>-1</sup>

The *Full Globe* (Fig. 2c) run uses the forcing composited over the entire globe to test the sensitivity of the response to a global forcing (anomalies are sparse beyond 45N and 45 S).

We note that a typical stationary Rossby wave train emanating from the tropics takes about 2 weeks to fully establish. Therefore, the North Pacific anomaly may be the response from a tropical forcing a few weeks prior, yet we composite the forcing using using the simultaneous heating in the region analyzed for a specific month/MJO phase/ENSO phase combination to examine the interference. The issue of a time-varying response due to the time it takes the Rossby wave to fully establish is beyond the scope of this study and would be better suited for the time-integration version of the LBM. The focus of this study is to analyze the spatial structure of the remote response to an imposed forcing derived from the realistic MJO-associated heating anomalies.

The experiments revealed that the teleconnection response *is* sensitive to the domain of the forcing (Fig. 3). The *Full Globe* (Fig. 3c) response shows an eastward shifted positive anomaly, starting in the eastern North

Pacific in P23, moving southeast to the central-west North Pacific in P45, the positive height stretches into the west coast of the U.S. in P67, then shifts further east to the southern U.S. in P81. This pattern can only be seen when the model is forced including the both the tropical and extratropical forcing.

Furthermore, the results show that the LBM is sensitive to fluctuations in the forcing used, seen in the variability of the response based on MJO phase, regardless of the forcing domain. For example, in both the *MJO Domain* and *Full Globe* responses (Fig. 3a,c), the western North Pacific positive height anomaly in P23 switches to a negative anomaly is 45, shifts eastward in P67, and switches back to a positive anomaly in P81.

The forcing domain sensitivity in also seen in the North American response pattern. In P23, when the LBM is forced with just the tropical forcing in the *MJO Domain* experiment (Fig. 3a), the subtropical Pacific has a strong negative anomaly centered over Hawai'i and a positive anomaly in the North Pacific, with a very weak response in the U.S. However, when the extratropical forcing is included for the *Full Globe* (Fig. 3c) experiment,



### **MJO Domain** North Pacific Only **Full Globe** a) c) 60N 60N 45N 45N 45N 30N Phases 2&3 Phases 2&3 Phases 2&3 120E 140E 160E 180 160W 140W 120W 100W 80W 140E 160E 180 160W 140W 120W 100W 80W 60W 140E 160E 180 160W 140W 120W 100W 80W 120E 60N 60N 60N 45N 45N 45N 301 30N 30N Phases 4&5 Phases 4&5 Phases 4&5 180 160W 140W 120W 100W 80W 60W 120E 140E 160E 180 160W 140W 120W 100W 80W 140E 160E 140E 160E 180 160W 140W 120W 100W 80W 60N 60N 60N 45N 45N 45N 30N 30N 30N Phases 6&7 Phases 6&7 Phases 6&7 160W 140W 120W 100W 80W 120F 140F 160F 180 120E 140E 160E 180 160W 140W 120W 100W 80W 140E 160E 180 160W 140W 120W 100W 80W 60N 60N 60N 45N 45N 45N 30N 30N 30N Phases 8&1 Phases 8&1 Phases 8&1 120E 140E 160E 180 180 160W 140W 120W 100W 80W 160W 140W 120W 100W 80W 60W 180 160W 140W 120W 100W 80W 120E 140E 160E -1 -0.75 -0.5 -0.25 0 0.25 0.5 0.75 1.25 1.5 meters

LBM El Niño Days Forcing and Base State

Fig. 3 The anomalous 500 mb geopotential height response from the LBM for the three forcing domains during El Niño days. Each panel consists of the weighted average of the monthly response from November to April

the positive anomaly in the North Pacific is maintained, while the negative anomaly is shifted eastward, extending over the continental U.S. In P45, the tropical forcing only produces a slightly positive anomaly over the US, while the tropical and extratropical forcing produced a negative height anomaly over the majority of the U.S. There is also a slight eastward shift in the response by including the North Pacific forcing. Overall, the response in the western subtropical and western North Pacific is dominated by the tropical forcing. The eastern subtropical Pacific and eastern North America are dominated by the extratropical forcing, where there is likely a downstream response from advection by the zonal winds.

The same set of domain-varying experiments were run for La Niña days (Fig. 4). The forcing domain sensitivity test results for the MJO forcing during La Niña days are similar to those for El Niño days, especially in that the inclusion of the North Pacific anomaly affects the response over North America. Without the inclusion of the Northern Hemisphere forcing (above 25N), the response is dominated by the MJO region forcing. When the Northern Hemisphere forcing (above 25N) is included, the North American response is dominated by the Northern Hemisphere forcing. Therefore, the LBM response is sensitive to the domain forcing and further suggests that the response over North America is sensitive to both a tropical and midlatitude forcing.

### **4 AGCM experiments**

The AGCM is run to compare the teleconnection response to both those in the LBM and the Reanalysis. Following a similar methodology used for the LBM, the model is forced with the diabatic heating anomalies over the (1) MJO Domain forcing domain and (2) the Full Globe forcing domain. Both forcing domains are tested here to examine if the tropical forcing alone dominates the midlatitude pattern, or if the full tropical-extratropical anomalous heating is necessary for capturing the midlatitude teleconnection pattern. The North Pacific Only forcing domain was not used for the AGCM.

There is strong sensitivity in the system to the MJO forcing based on phase, meaning the AGCM Northern Hemisphere response to the tropical forcing is sensitive to the



30N

-1.75 -1.5 -1.25

Phases 8&1

120E 140E 160E

### LBM La Niña Days Forcing and Base State North Pacific Only a) **MJO Domain** c) Full Globe 60N 60N 60N 45N 45N 30N 30N 30N Phases 2&3 Phases 2&3 Phases 2&3 180 160W 140W 120W 100W 80W 60W 180 160W 140W 120W 100W 80W 60W 120F 140F 160F 180 160W 140W 120W 100W 80W 60W 120E 140E 160E 120E 140E 160E 60N 60N 45N 45N 45N 30N 30N 30N Phases 4&5 Phases 4&5 Phases 4&5 180 160W 140W 120W 100W 80W 60W 120E 140E 160E 180 160W 140W 120W 100W 120E 140E 160E 180 160W 140W 120W 100W 80W 120E 140E 160E 80W 60N 60N 60N 45N 451 30N Phases 6&7 Phases 6&7 Phases 6&7 120E 140E 120E 140E 160E 180 160W 140W 120W 100W 80W 60W 160W 140W 120W 100W 80W 60W 140E 160E 180 160W 140W 120W 100W 80W 60W 120E 60N 60N 60N 45N 45N 45N

## Fig. 4 The anomalous 500 mb geopotential height response from the LBM for the three forcing domains during La Niña days. Each panel consists of the weighted average of the monthly response from November to April

meters

180 160W 140W 120W 100W 80W 60W

-1 -0.75 -0.5 -0.25 0 0.25 0.5 0.75 1 1.25 1.5 1.75

location and domain of the MJO forcing, which generally supports the conclusions drawn from the LBM experiments. In Fig. 5, the 500 mb geopotential height response from the AGCM is shown for the *MJO Domain* forcing experiment (left) and the *Full Globe* forcing experiment (right) for El Niño days. Figure 6 shows the same, but for La Niña days.

301

Phases 8&1

120E 140E 160E 180 160W 140W 120W 100W 80W 60W

The AGCM results from the *MJO Domain* run for El Niño days show a positive height anomaly over the Northwest Pacific in P23 that remains fairly stagnant through P81. There is a negative height anomaly over Northwest Canada in P23 that expands to covering Alaska and the Northwest Pacific in P45, then returns to a similar structure as in P23 for P67 and P81. There is also a weak positive anomaly to the east of North America in P23 that expands to the entire southern U.S. in P67.

The AGCM *Full Globe* forcing domain response for El Niño days differs slightly from the *MJO Domain* run in all phases, although the general structure of the response is similar, particularly in P45 and P81. In P23, the *Full Globe* response is shifted eastward, while the P45 response is similar between the two forcing runs, but the negative height anomaly spans less area in the *Full Globe* response. In P67,

a large positive height anomaly is found over the entirety of North America with a center over California, and no negative height anomaly is found in Canada as in the *MJO Domain* run.

30N

Phases 8&1

120E 140E 160E

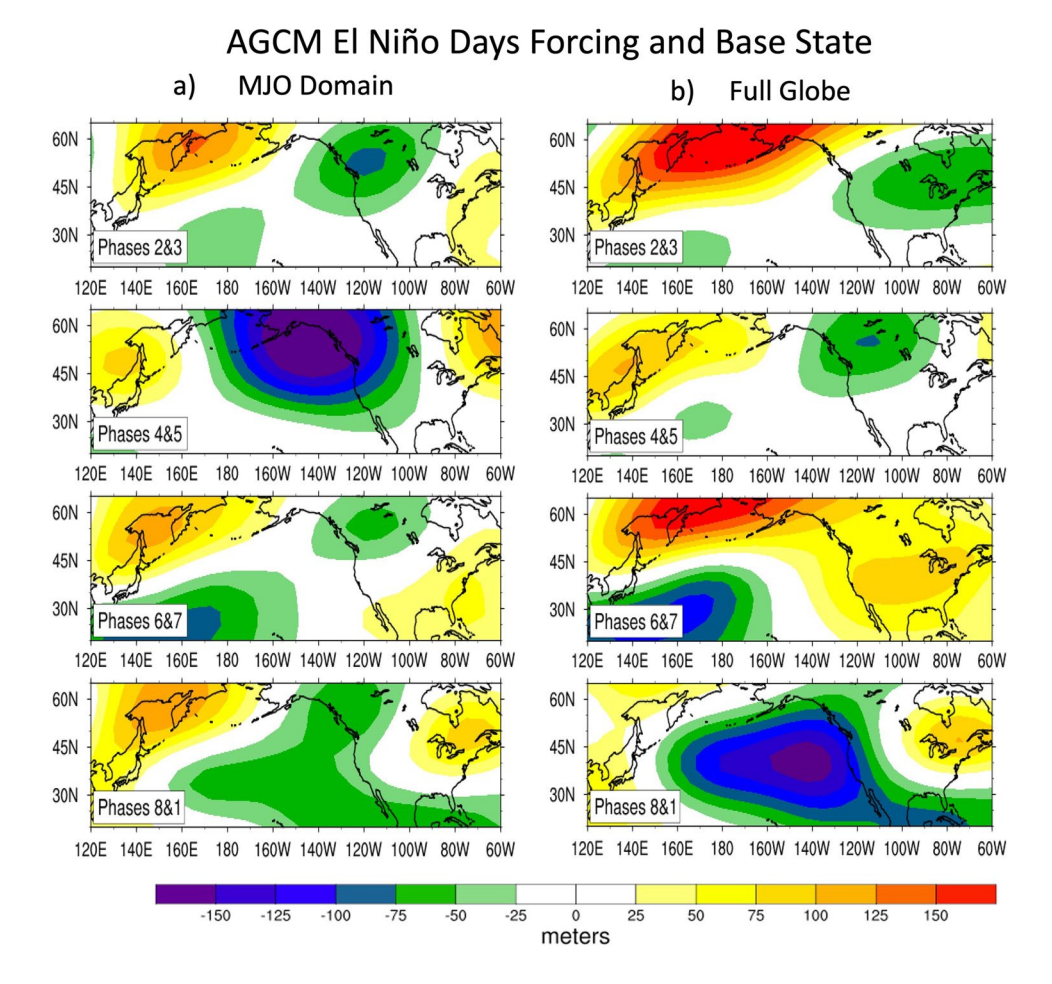
180 160W 140W 120W 100W 80W 60W

The AGCM responses differ from the LBM responses in that the *Full Globe* LBM run responses are simply a summation of the tropical forcing response and the North Pacific forcing response, while the AGCM responses are not, due to the nonlinear nature of the AGCM. The LBM responses for both domain forcing experiments show symmetry in the MJO phases in that P23 and P67 and P45 and P81 show nearly opposite identical patterns, while this contrast is not found in the AGCM results.

The La Niña day results in Fig. 6 show that the *MJO Domain* and *Full Globe* forcing domain responses are similar in structure for P67 and P81, but P23 and P45 show very different responses. The *MJO Domain* forcing domain response is similar to the El Niño days responses with a positive height anomaly over the western North Pacific and a negative anomaly over the eastern North Pacific and Canada in P23 and a large negative anomaly spanning the North Pacific in P45. However, in the *Full Globe* forcing



Fig. 5 The anomalous 500 mb geopotential height response during El Niño days from the AGCM for the MJO Domain forcing domain experiment (left) the Full Globe forcing domain experiment (right). Each panel consists of the weighted average of the monthly response from November to April



domain response, the negative anomalies in P23 and P45 are small and there is an eastward shifted positive height anomaly from P23 to P45.

### 5 ENSO-modulation of MJO teleconnections

The models' abilities to capture the Northern Hemisphere teleconnection pattern is assessed by comparing the models' outputs to each other and to reanalysis. For conciseness, an MJO forcing composited during El Niño, La Niña, or Neutral days will be referred to as an El Niño MJO forcing, La Niña MJO forcing, or ENSO Neutral days forcing, respectively.

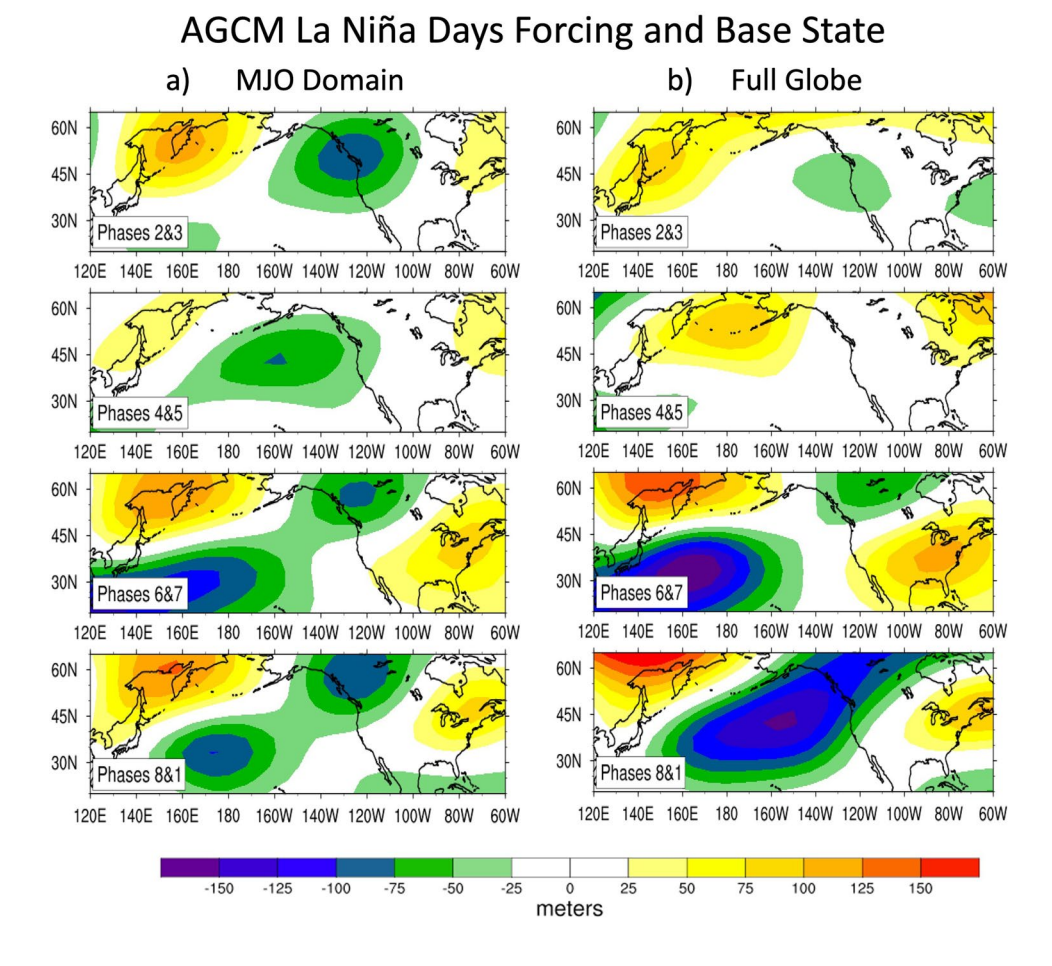
First, ENSO modulation of the MJO-associated diabatic heating calculated from reanalysis (Eq. 1) is analyzed. The top left panel (Fig. 7a) shows the MJO-associated diabatic heating anomalies composited over the November–April days during which an MJO was active and in P23 during El Niño days. The top center panel (Fig. 7b) shows days composited using the same criteria but during La Niña days. The top right panel (Fig. 7c) shows the same but for ENSO Neutral days. The same method continues for MJO P45, P67,

and P81. The La Niña MJO forcing is stronger than the El Niño MJO forcing over the Indian Ocean in P23 and over the Maritime Continent in P45. Differences in the forcing are also seen in the North Pacific with a stronger negative forcing (cooling) during La Niña in P45. There is also a strong warming in the subtropical Pacific near Hawai'i during La Niña in P81 that is not seen during El Niño. The heating and cooling magnitude of the MJO forcing during La Niña is generally stronger. Overall, the MJO forcing is clearly modulated in both location and magnitude by the ENSO base state.

To assess if ENSO phase affects the teleconnection response associated with the MJO in reanalysis estimates, we look at reanalysis 500 mb geopotential height anomalies (Fig. 8) with the zonal-mean removed for direct comparison to the LBM and AGCM results for both El Niño and La Niña days. The panels correspond to the same days composited as in Fig. 7a,b. For both El Niño and La Niña days, the anomalous 500 mb geopotential height has a wave train pattern spanning from the North Pacific to over North America. The primary differences in the height patterns during El Niño versus La Niña days are in the eastward extent of the North Pacific height anomaly and the height structure over North



Fig. 6 The anomalous 500 mb geopotential height response during La Niña days from the AGCM for the MJO Domain forcing domain experiment (left) the Full Globe forcing domain experiment (right). Each panel consists of the weighted average of the monthly response from November to April



America. In general, the North Pacific anomaly shifts east-ward during El Niño, but shrinks and remains stationary during La Niña. There is a more pronounced and larger eastern U.S. anomaly during La Niña than El Niño. If there was little to no difference in the MJO-associated anomalous height pattern between the El Niño days and the La Niña days, it would imply that the extratropical teleconnection pattern associated with the MJO was independent of ENSO phase. However, there are clear differences that vary spatially and by MJO phase which provides strong evidence for the modulation of MJO teleconnections by ENSO. These results are consistent with Moon et al. (2011), who note shifted extratropical anomalies during El Niño and La Niña periods.

The LBM does capture differences in the responses during El Niño versus La Niña, suggesting that the variations in the base state and forcing due to ENSO impact the MJO teleconnections in this linear framework. A comparison of Figs. 3c and 4c shows that during La Niña days, the anomalous height patterns in the North Pacific extend more into the U.S. than during El Niño days. In the LBM response, the North Pacific height patterns for both positive and negative anomalies have larger magnitudes during La Niña, particularly in P23 and P67. Differences in the Northern Hemisphere response patterns span the North Pacific and North

America and are highly variable when considering El Niño versus La Niña modulation.

To quantify how much of the teleconnection pattern associated with the MJO is captured by the LBM, we calculate the centered Pearson product-moment coefficient of linear correlation (adopted from the skill metrics from Wang et al. (2020a)) between the LBM and AGCM output for the *Full Globe* run and the Reanalysis. We compute the correlation for each MJO phase over the Northern Pacific-North American region (20N–65N; 120E–300E). The results are summarized in Table 2 (top).

The LBM generally reproduces the teleconnection pattern seen in Reanalysis over the North Pacific—a positive height anomaly in P23 and P45 and a negative height anomaly is P67 and P81. This suggests that linear dynamics are sufficient, at least in part, in capturing the teleconnection pattern over the North Pacific. P67 overall has the highest pattern correlation between the model response and Reanalysis. However, much of the teleconnection pattern over the U.S. in Reanalysis is not accurately reproduced by the LBM, suggesting that linear dynamics are insufficient in capturing the full teleconnection response over the U.S. Further, for most MJO phases except P23, more of the teleconnection pattern seen in Reanalysis is captured by the LBM during La Niña



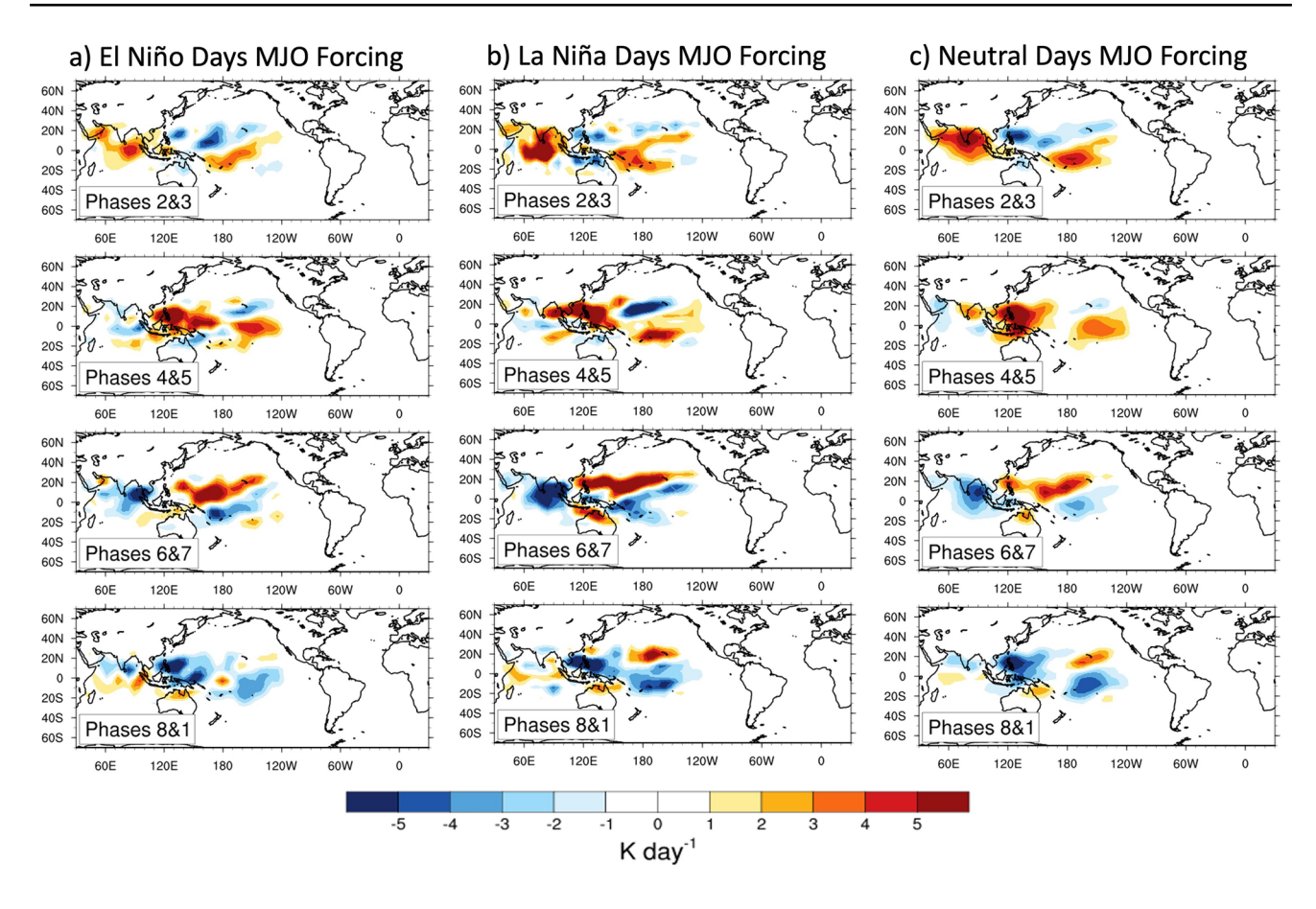


Fig. 7 a The MJO-associated anomalous 700 mb diabatic heating composited based on a November–April weighted monthly average and MJO phase during a El Niño days, b La Niña days, c ENSO Neutral days. Units are K day<sup>-1</sup>

days than El Niño days with the *Full Globe* forcing, but vice versa for the *MJO Domain* forcing.

Next, the results from the AGCM experiments are discussed and compared to the results from the LBM and Reanalysis. The AGCM Full Globe forcing domain response for El Niño days (Fig. 5b) differs slightly from the MJO Domain (Fig. 5a) run in all phases, although the general structure of the response is similar, particularly in P45 and P81. In P23, the Full Globe response is shifted eastward, while the P45 response is similar between the two forcing runs, but the negative height anomaly spans less area in the Full Globe response. In P67, a large positive height anomaly is found over the entirety of North America with a center over California, but no negative height anomaly is found in Canada as in the MJO Domain run. The La Niña day results in Fig. 6 show that the MJO Domain and Full Globe forcing domain responses are similar in structure for P67 and P81, but P23 and P45 show very different responses. The MJO Domain forcing domain response is similar to the El Niño days response with a positive height anomaly over the Northwest Pacific and a negative anomaly over the Northeast Pacific and Canada in P23 and a large negative anomaly spanning the North Pacific in P45. However, in the *Full Globe* forcing domain response, the negative anomalies in P23 and P45 are small and there is an eastward shifted positive height anomaly from P23 to P45.

Overall, the responses from the AGCM Full Globe forcing domain closer resemble the wave train height pattern seen in Reanalysis for both El Niño and La Niña days in the North Pacific and North Pacific America than the LBM. This suggests that the simultaneous MJO-associated anomalies in the tropics and the diabatic heating anomalies in the midlatitudes are important for the structure of the Northern Hemisphere teleconnection response to the MJO forcing. Table 2 (bottom) shows the centered Pearson correlation coefficients between the AGCM 500 mb geopotential height response output and Reanalysis MJO-associated 500 mb geopotential height anomalies. The AGCM modestly captures more of the teleconnection response seen in Reanalysis over North America especially when forcing the model with a Full Globe forcing, which supports the hypothesis that the North American teleconnection response to the MJO forcing has a significant nonlinear component. We note that the



Fig. 8 a The NCEP-NCAR Reanalysis 500 mb geopotential height MJO-associated anomalies during El Niño days broken down by MJO phase. b Same as a but for La Niña days

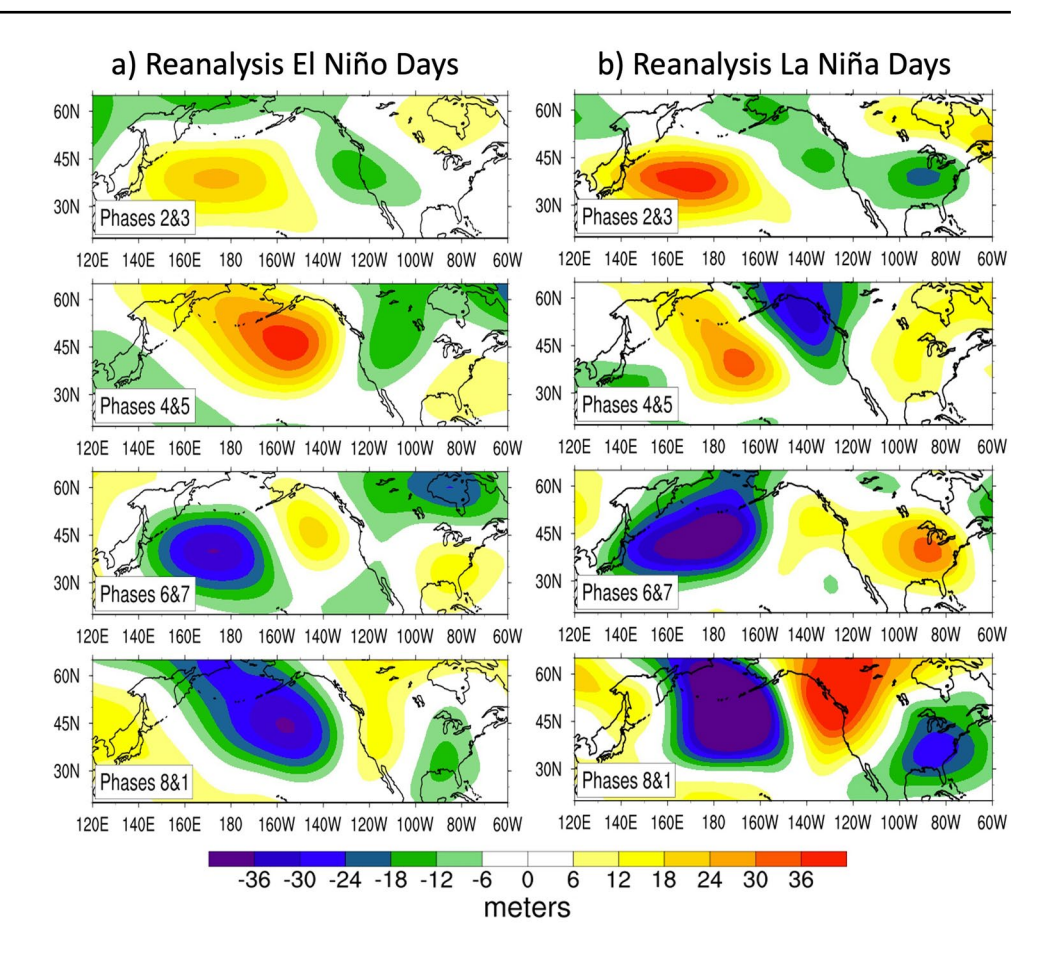


**Table 2** Pearson correlation coefficients (centered) between the 500 mb anomalous geopotential height in Reanalysis and the 500 mb geopotential height LBM response (top) and AGCM response (bot-

tom) for the Full Globe forcing domain experiment for El Niño days (left) and La Niña days (right)

El Niño days rea	nalysis versus LBM output patte	ern correlation coefficient	La Niña days reanalysis versus LBM output pattern correlation coefficient					
	MJO domain forcing	Full globe forcing		MJO domain forcing	Full globe forcing			
MJO P23	0.13	0.34	MJO P23	0.00	0.24			
MJO P45	0.33	0.12	MJO P45	0.27	0.19			
MJO P67	0.54	0.30	MJO P67	0.32	0.52			
MJO P81	0.02	- 0.22	MJO P81	0.29	0.19			
El Niño days rear	nalysis versus AGCM output pa	attern correlation coefficient	La Niña days reanalysis versus AGCM output pattern cor- relation coefficient					
	MJO domain forcing	Full globe forcing		MJO domain forcing	Full globe forcing			
MJO P23	- 0.15	- 0.10	MJO P23	- 0.08	0.04			
MJO P45	- 0.38	0.32	MJO P45	- 0.13	0.49			
MJO P67	0.46	0.53	MJO P67	0.21	0.39			
MJO P81	0.05	0.41	MJO P81	- 0.08	0.15			

The correlation coefficients are computed for each MJO phase and computed over the entire Northern Pacific-North American region (20N-65N; 120E-300E)



coefficients are computed over the full North Pacific-North American region for a substantial number of grid points to be included in the spatial correlation calculation. While the the Pearson correlation coefficients are not uniformly higher for the AGCM responses compared to the LBM responses, the AGCM produces more of the wave-train pattern seen in Reanalysis and the response over North America than the LBM.

Differences in the spatial pattern of the AGCM responses between El Niño days and La Niña days for the MJO Domain forcing domain and the Full Globe forcing domain (Figs. 5, 6) highlight that ENSO is modulating the MJOassociated teleconnection response in the AGCM and these differences vary by MJO phase, which was also seen in the LBM results (Figs. 3, 4). There are larger differences in the Full Globe domain responses than the MJO Domain, particularly in P23 and P67 which confirms the results that a forcing in the midlatitudes impacts the North American teleconnection response. While neither the LBM or AGCM fully capture the teleconnection response to the MJO forcing during El Niño and La Niña seen in Reanalysis, the differences in the response patterns suggest that the base state and forcing based on ENSO phase play a role in the modulation of the teleconnection pattern.

### 5.1 Rossby wave source analysis

To analyze the physical mechanisms underlying the ENSO modulation of the MJO teleconnections in the modeling framework, we analyze the so-called Rossby wave source term. This term is derived from the linearized barotropic vorticity equation (Sardeshmukh and Hoskins 1988) and is given by

$$S' = -\nabla \cdot \left( \overline{\zeta} \, \mathbf{v}_{\chi}' + \overline{\mathbf{v}}_{\chi} \, \zeta' \right) \tag{3}$$

where S is the Rossby wave source term,  $\zeta$  is the absolute vorticity and  $\mathbf{v}_{\chi}$  is the divergent component of the wind, and the overbar represents climatology and the prime represents anomalies. The Rossby wave source term is useful for locating the origin or source of anomalous Rossby waves via advection and stretching of the climatological absolute vorticity by the anomalous divergent flow (first term) and advection and stretching of the anomalous absolute vorticity by the climatological divergent flow (second term). It characterizes the relationship between the upper level divergent flow in regions of strong convection (e.g. tropics) and the remote circulation response in regions with a strong background vorticity gradient (e.g. subtropics and midlatitudes) (Tseng et al. 2020; Lopez et al. 2016).

The Rossby wave source (RWS) term was calculated for the AGCM response for the El Niño days and La Niña days P23 and P67 MJO forcing for both the MJO Domain and the Full Globe domain shown in Fig. 9. In P23, the RWS from an MJO Domain forcing exhibits an east-west dipole structure over the Asian continent, while in P67, the RWS structure has more of a north-south structure, particularly during El Niño days. During La Niña days, the RWS structure is more zonally extended with higher magnitudes, consistent with Tseng et al. (2020) who also found the dipole structure varies based on MJO phase and the RWS pattern is weakened during MJO forcings during El Niño years. For El Niño and La Niña days with the MJO Domain forcing, the RWS extends across the North Pacific and into North America during P23, but the RWS is much weaker in P23 for the Full Globe Domain forcing. However, the opposite holds true during P67 in which the RWS does not extend across the North Pacific-North American sector with the MJO Domain forcing, but does extend with the Full Globe Domain forcing. This is evident in the weak AGCM responses for the Full Globe forcing in P23, particularly during La Niña days (see Figs. 5b and 6b), suggesting that heating anomalies in the subtropics influence Rossby wave propagation. ENSO is found to modulate the structure and magnitude of the RWS as well as the eastward extent of the Rossby wave propagation.

# 5.2 Role of ENSO-modulated base state versus ENSO-modulated forcing on teleconnection pattern

The question then remains of whether the base state or the MJO-associated forcing is the dominant driver of the changes in the teleconnection patterns during an El Niño versus La Niña. To test this, a series of Swap Test experiments were conducted in both models in which the base states are swapped from the respective ENSO phase to a neutral ENSO phase base state for both El Niño and La Niña MJO forcing. Conversely, an ENSO Neutral days forcing was used with an El Niño and La Niña days NDJFMA base state, respectively. The MJO Domain domain was used for both the El Niño days and La Niña days forcing to test direct modulation of the MJO forcing. The first experiment (Fig. 10a) used the El Niño MJO forcing imposed on the ENSO Neutral base state, and the second experiment (Fig. 10b) used the La Niña MJO forcing imposed on the ENSO-neutral base state. The third (Fig. 10c) used an ENSO Neutral forcing with an El Niño climatological base state and the fourth (Fig. 10d) used an ENSO Neutral forcing with a La Niña climatological base state. The overall structure of the response pattern is more closely related to the response pattern with the corresponding forcing, i.e. the El Niño MJO forcing during the ENSOneutral base state more closely resembles the El Niño MJO forcing and El Niño base state than the ENSO neutral forcing with an El Niño base state. The same holds that the La



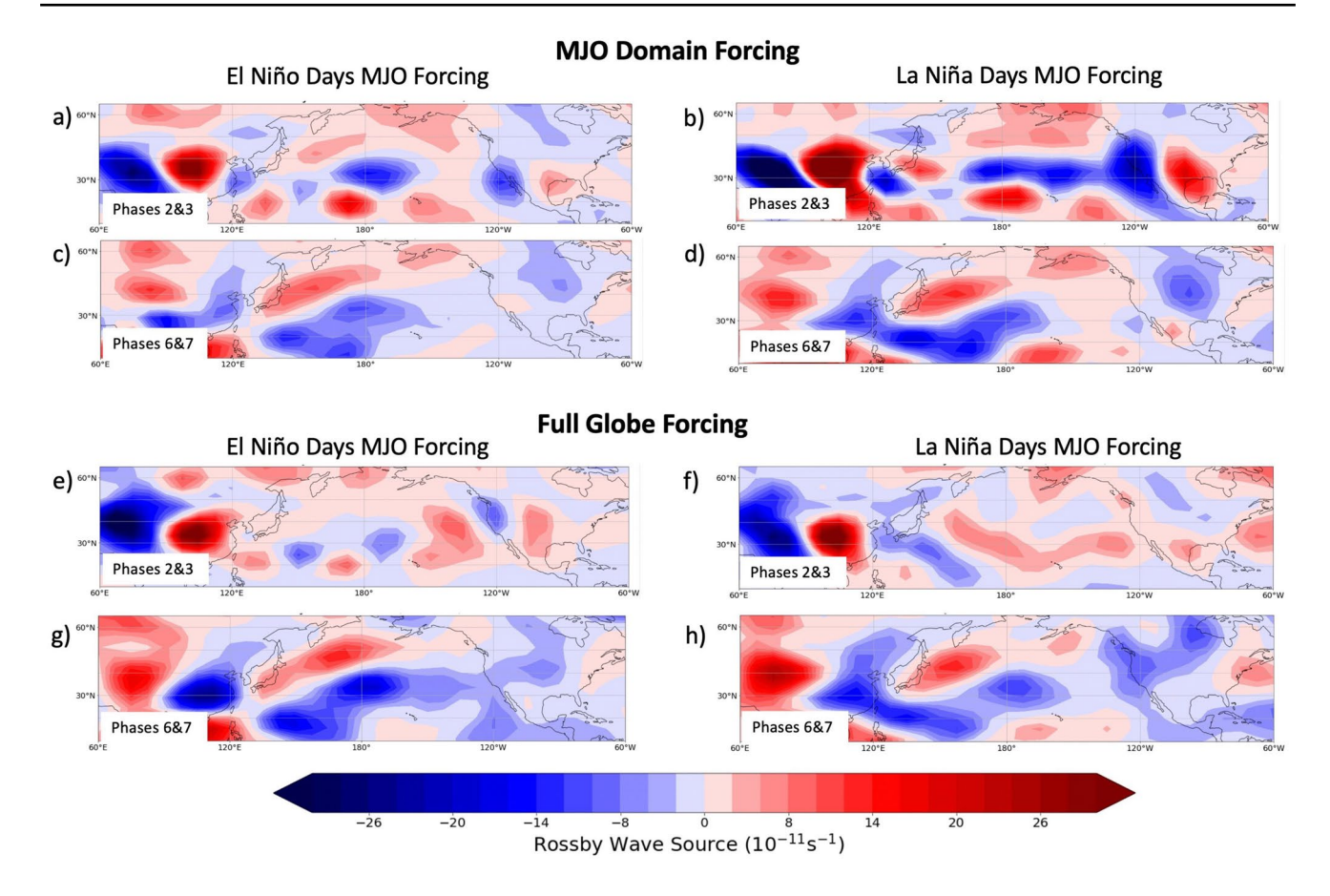


**Fig. 9** (Top) Rossby Wave Source Term  $(10^{-11} \text{ s}^{-1})$  calculated using the *MJO Domain* forcing for El Niño days during P23 (**a**) and P67 (**c**) and for La Niña days during P23 (**b**) and P67 (**d**). (bottom) The

Rossby Wave Source Term calculated using the *Full Globe* Domain forcing for El Niño days during P23 (e) and P67 (g) and for La Niña days during P23 (f) and P67 (h)

Niña MJO forcing with an ENSO-neutral base state more closely resembles the La Niña forcing with a La Niña base state than the ENSO neutral forcing with an La Niña base state. Thus, variations in the forcing produce larger changes than variations in the base state, indicating that the ENSO-modulated MJO forcing has a larger influence on teleconnection response than the base state.

A similar set of *Swap Test* experiments were performed to determine if the results from the LBM held true in the AGCM. The results are shown in Fig. 11 and the results are consistent with the *Swap Test* results from the LBM. The midlatitude teleconnection responses resemble the general structure of the ENSO-phase based on the forcing more than the base state, which confirms the LBM results that the MJO-forcing modulated by the ENSO background state is dominating the Northern Hemisphere teleconnection response. Additionally, the ENSO Neutral forcing runs with the El Niño and La Niña base state (Fig. 11c, d) are virtually indistinguishable while the ENSO Neutral base states forced with the El Niño and La Niña (Fig. 11a, b) have clear differences, as the forcing plays a larger role in the response than the base state in these modeling frameworks. Previous studies have also shown the importance

of the base state in reproducing MJO teleconnections and that biases in base state can lead to biases in MJO teleconnections (Henderson et al. 2017; Wang et al. 2020b). The modeling experiments in this study extend these results to directly compare the role of the base state and the forcing, and while both the base state and the forcing need to be accurately represented to produce MJO teleconnections, these experiments show that the MJO forcing that has been modulated by the ENSO background state creates larger differences in the response patterns than the base state alone.

Finally, a series of experiments were run in both models in which the base state month was held constant (i.e. January, MJO P45, El Niño days) while the forcing month was rotated (i.e. November–April, MJO P45, El Niño days) and vice versa for the forcing month being held constant while the base state month was rotated. Results in both models (not shown) reveal that the models were much more sensitive to a change in the monthly forcing than a change in the monthly base state. This further confirms that the ENSO-modulated MJO forcing has larger influence on the teleconnection pattern than the base state.



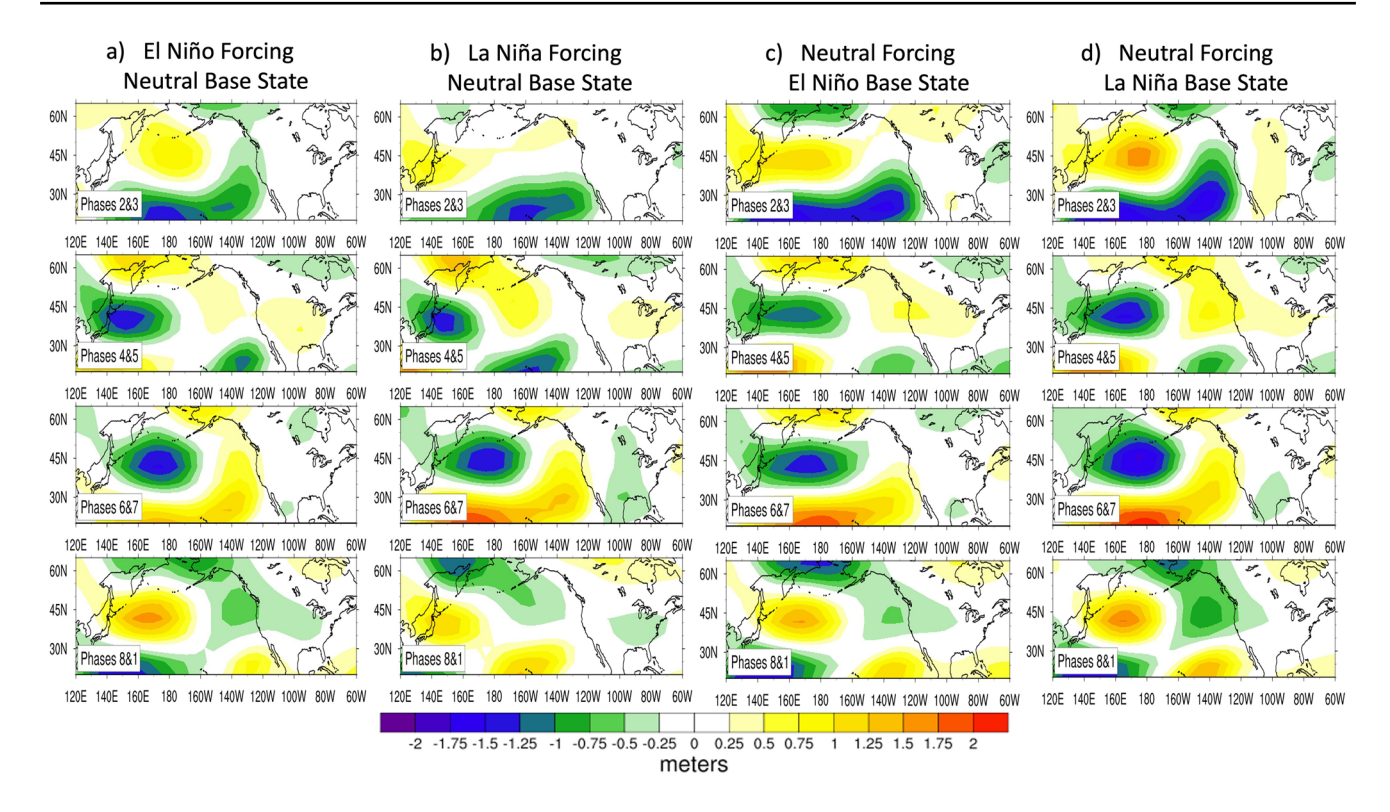


**Fig. 10** LBM Swap Test Experiment: The 500 mb geopotential height response from the LBM experiments using the MJO Domain forcing domain. **a** shows the response from forcing the LBM with the MJO-associated diabatic heating during El Niño days with an ENSO Neutral climatological base state; **b** shows the LBM response to a La Niña days forcing with an ENSO Neutral climatological base state; **c** 

shows an ENSO Neutral days forcing with an El Niño climatological base state; **d** shows an ENSO Neutral days forcing with a La Niña climatological base state. Each panel is a weighted average of the number of day from each month November–April used for the forcing composite during that specific MJO phase

### 6 Conclusions and summary

ENSO is known to modify the base state through which the MJO is propagating as well as the MJO itself (Pohl and Matthews 2007), but what is not fully understood is the role that ENSO plays in modulating the MJO teleconnection pattern in the Northern Hemisphere. A linear baroclinic model (LBM; Watanabe and Kimoto 2000) and a dry atmospheric general circulation model (AGCM; Kirtman et al. 2001) are employed to assess how much of the MJO-associated teleconnection response can be captured with linear and nonlinear dynamics, respectively. We additionally look to pinpoint the most important aspects of the role of ENSO in modulating the extratropical teleconnection response to the tropical forcing.

Base states are composited based on ENSO state climatology for November–April. The MJO forcing used in the model are composited based on three conditions: boreal winter month (November–April), MJO phase (P23, P45, P67, or P81), and ENSO phase (El Niño, La Niña, or ENSO Neutral). While the models used are simplified, this study uses a forcings that are both subseasonal and realistic in a 2-tier climate model hierarchy.

The extratropical response is assessed first via experiments in which the LBM is forced with an MJO-associated forcing. Results show that the extratropical response is sensitive to changes in both the monthly MJO-associated forcing and the base state. Sensitivity testing also revealed that the MJO teleconnection response is sensitive to the domain of the forcing. The western and central North Pacific responses are dominated by the tropical location of the forcing, while the eastern Pacific and North American responses are dominated by the subtropical forcing.

The Northern Hemisphere anomalous 500 mb geopotential height teleconnection pattern associated with the MJO in Reanalysis is partly captured in the LBM in the North Pacific, but is not well captured in North America. Overall, the results suggest the teleconnection response over the North Pacific is at least partly a direct linear response to the MJO-associated forcing, but the teleconnection response over North America is more complex.

While the LBM was not able to fully capture the MJOassociated anomalous geopotential height response in the Northern Hemisphere, a number of conclusions can still be drawn about the sensitivity of the MJO teleconnection response and the role of ENSO via the LBM experiments.



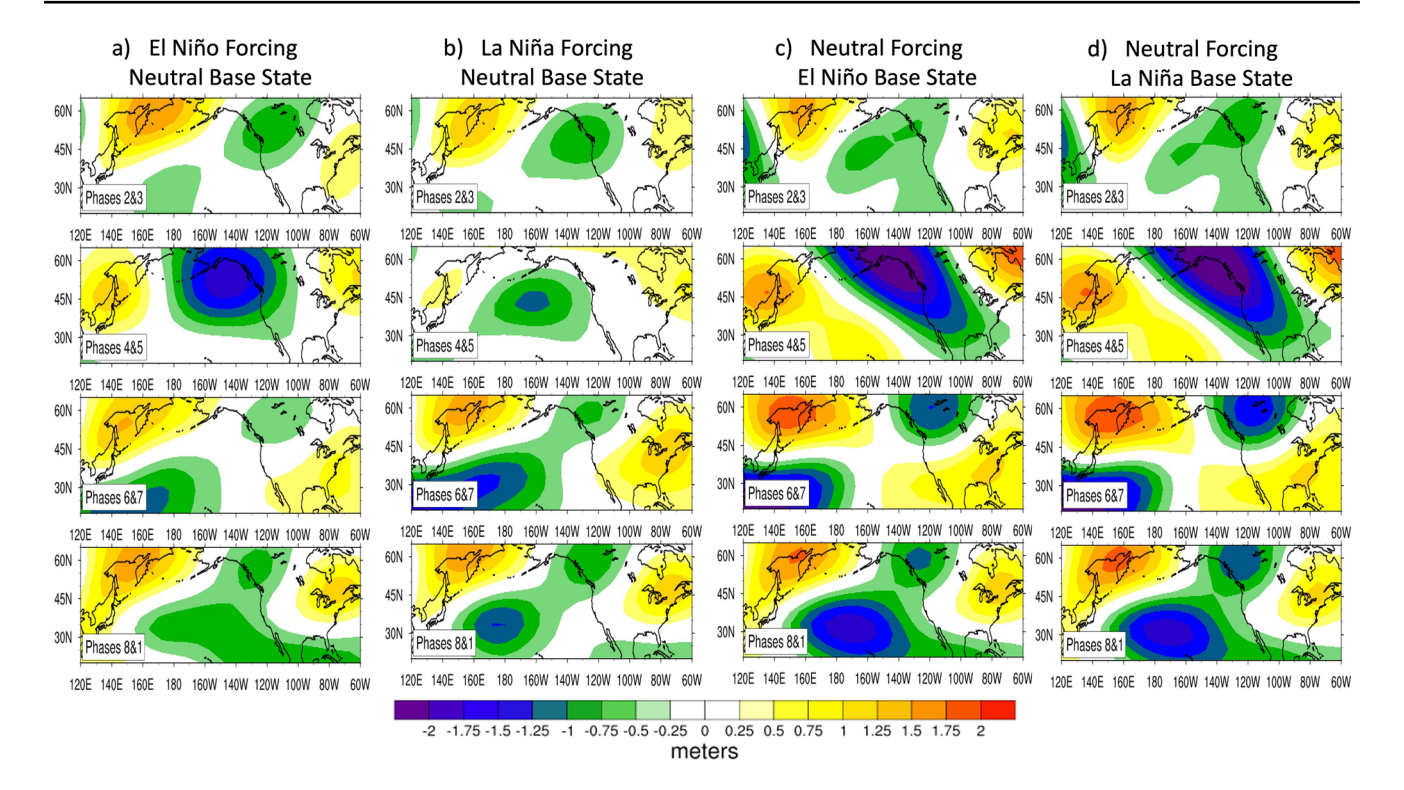


**Fig. 11** AGCM Swap Test Experiment: The 500 mb geopotential height response from the AGCM experiments using the MJO Domain forcing domain. **a** shows the response from forcing the AGCM with the MJO-associated diabatic heating during El Niño days with an ENSO Neutral climatological base state; **b** shows the AGCM response to a La Niña days forcing with an ENSO Neutral climato-

logical base state;  $\mathbf{c}$  shows an ENSO Neutral days forcing with an El Niño climatological base state;  $\mathbf{d}$  shows an ENSO Neutral days forcing with a La Niña climatological base state. Each panel is a weighted average of the number of day from each month November–April used for the forcing composite during that specific MJO phase

The LBM captures differences in the responses to MJO forcing during El Niño and La Niña, suggesting that the variations in the base state and forcing due to ENSO impact the MJO teleconnections. Differences in the Northern Hemisphere response patterns span the North Pacific and North America and are highly variable when considering El Niño versus La Niña modulation. Linear dynamics are sufficient in capturing differences between the Northern Hemisphere teleconnections associated with the MJO during El Niño and La Niña.

The next step in the model hierarchy was the use of a dry nonlinear atmospheric general circulation model (AGCM) to help understand the role nonlinear dynamics play in the ENSO-modulated MJO-induced teleconnection. The results from the AGCM are analyzed and compared to the results from the LBM to draw conclusions about the importance of incorporating nonlinear dynamics for modeling MJO teleconnections.

The AGCM uses the same climatological ENSO base states as the LBM and forcings that are composited over the same days as the LBM forcings following the same triply conditional criteria: month, MJO phase and ENSO phase. A weighted average of the monthly responses is

calculated to assess the AGCM teleconnection response for MJO phases for El Niño and La Niña days.

The results show that the Northern Hemisphere teleconnection response to MJO-associated forcing is sensitive to the MJO phase and the forcing domain. The AGCM Full Globe domain forcing runs capture more of the general teleconnection pattern wave train in the Northern Hemisphere than the LBM Full Globe domain forcing runs, implying that nonlinear dynamics better represent the teleconnection pattern than linear dynamics alone. Further, nonlinear dynamics are necessary in producing the North American height response since the AGCM captures more of the variability over North America than the LBM. While some features are better resolved by the nonlinear model, in general there are important features of observational estimates that are missed in both models. Results from both models shows that ENSO is modulating the MJO-associated teleconnection responses since the quasi-stationary Rossby wave train set up by the heating associated with the MJO is altered due to the ongoing ENSO phase, which in turn alters the teleconnection response. A Rossby wave source analysis reveals ENSO modulation of the structure and magnitude of the Rossby

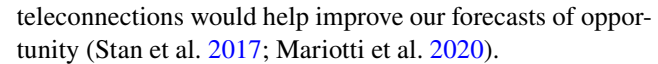


wave source term in the subtropics, particularly over the Asian continent and the West Pacific.

The modeling experiments also reveal that changes to the base state and the MJO forcing itself due to modulation via ENSO produce different teleconnection patterns in North America. This further strengthens the argument that subseasonal teleconnections associated with the MJO should be considered separately for El Niño and La Niña events. ENSO is not only modulating the base state, but it is modulating the forcing associated with the MJO, which dominates the response in varying teleconnection patterns in the Northern Hemisphere. The LBM and AGCM experiments both show that the MJO-forcing has a larger influence over the teleconnection pattern than the base state. Thus, it is the modulation of the MJO diabatic heating (convection) by ENSO that dominates the ENSO-phase-dependent changes to the Northern Hemisphere teleconnection pattern.

### 7 Discussion

The present study analyzes MJO teleconnections through the lens of the ENSO background state. Other factors are known to influence the MJO on internannual and longer timescales, such as the OBO (Collimore et al. 2003; Liess and Geller 2012; Yoo and Son 2016). Studies have shown that the QBO affects MJO amplitude, particularly in boreal winter, with enhanced MJO teleconnection patterns during QBO easterly phases than westerly phases (Yoo and Son 2016; Son et al. 2017) which can lead to more predictable SSW events (Liu et al. 2014) and behavior in the extratropics (Mayer and Barnes 2020). The QBO has also been found to impact MJO propagation (Densmore et al. 2019; Hendon and Abhik 2018) and persistence (Lim et al. 2019) with year-to-year variation of the subseasonal convective activity being dominated by the QBO (Son et al. 2017). Further, there is potential for an asymmetry in the relationship between the QBO and ENSO in that the QBO can affect frequency of ENSO events (Nishimoto and Yoden 2017), which could impact the frequency of certain Northern Hemisphere teleconnection patterns. Additional studies could further address how the MJO and its associated teleconnection patterns are modulated by both ENSO and the QBO simultaneously. For example, a similar approach to Liess and Geller (2012) which separated the QBO signal from the ENSO signal and applied in Nishimoto and Yoden (2017) for ENSO-neutral years could be extended to additionally separate the MJO signal. To address cold and warm phases of ENSO this would reduce sample size of days fitting the necessary criteria of MJO/ ENSO/QBO phase and would require a more intricate detangling of the processes and nonlinearities. A deeper understanding of multiple climate modes operating on varying temporal and spatial scales and their tropical-extratropical



The LBM does not reproduce the full Reanalysis 500 mb geopotential height pattern, likely due to a lack of nonlinear processes, particularly from transient eddies. Both the LBM and the dry AGCM lack diabatic heating feedbacks and moisture-convective feedbacks that are needed to better reproduce the observational estimates (Held et al. 1989; Hirota and Takahashi 2012; Wei and Ren 2019). While Mori and Watanabe (2008) show that the MJO-induced teleconnection is dominated by linear dynamics, the results from this study show that linear dynamics are not sufficient in fully capturing the full ENSO-modulated Northern Hemisphere teleconnection pattern, especially over North America. Including nonlinear dynamics via the AGCM improves some aspects of the teleconnection response, primarily the wave train pattern, but modestly. Future plans with the nonlinear AGCM include adding semi-stochastic processes in interactive heating in particular.

We note that there is a strong subtropical response in the LBM response that is not present in the AGCM output or the Reanalysis. While the understanding for this difference is beyond the scope of this study, we propose that nonlinearities and wave-wave interactions in the system are important for mixing and eddy stirring which could remove the relatively strong subtropical-midlatitude gradients and reduces the subtropical response.

The simplicity of both the LBM and AGCM allow for diagnoses of physical mechanisms by stripping away complex features such as moist processes, coupling between the ocean and the atmosphere, and imposing a propagating MJO. However, these features should be addressed when considering the full scope of the Northern Hemisphere MJO teleconnection patterns and included in additional climate model hierarchical experiments.

### **Appendix**

### **Anomalous diabatic heating derivation**

The following is the derivation for the conversion of precipitation into diabatic heating. The variables here are written as total variables, but taken as anomalies in Eq. 1.

We begin with the formula for total precipitable water, or for our purposes, precipitation (precip).

$$precip(x, y, t) = \int_0^\infty C(x, y, t, z) dz$$
 (4)

where C(p) is condensation in the water column, or the mixing ratio at pressure level p in g kg<sup>-1</sup>. Applying the hydrostatic equation,



$$\frac{\partial p}{\partial z} = -\rho g \tag{5}$$

where  $\rho$  is the density of water vapor, and g is the acceleration of gravity. The equation becomes

$$precip(x, y, t) = \frac{-1}{\rho g} \int_{p_s}^{0} C(x, y, t, p) dp$$
 (6)

where  $p_s$  is surface pressure. Integrating over the full column

$$precip(x, y, t) = \frac{p_s}{\rho g} C(x, y, t)$$
 (7)

From the thermodynamic energy equation approximation, we know that

$$\dot{Q}'(x,y,t) \sim \frac{L_{\nu}}{c_p} C(x,y,t) \tag{8}$$

where Q is diabatic heating,  $L_v$  is the latent heat of vaporization, and  $c_p$  is the specific heat of water. Substituting for C(x,y,t) in (4) and applying a distribution of the heating in the vertical, we find

$$\dot{Q}'(x,y,t,p) = \left(\frac{L_{\nu}\rho g}{c_{p}p_{s}}\right) (precip(x,y,t))(\eta(p))$$
(9)

where  $\eta(p)$  is the normalized vertical structure such that

$$\int_0^{p_s} \eta(p)dp = 1 \tag{10}$$

or in another form

$$\eta(p) = \frac{\hat{\eta}(p)}{\int_0^{p_s} \hat{\eta}(p) \, dp}.\tag{11}$$

The measurements used for Eq. 1 are as follows:

- $L_v = 2,260,000 \text{ J kg}^{-1}$ ; latent heat of vaporization
- $\rho = 1.0 \text{ kg m}^{-3}$ ; density of air integrated over column
- $g = 9.8 \text{ m s}^{-2}$ ; acceleration of gravity
- $c_p = 4186 \text{ J kg}^{-1} \text{ K}^{-1}$ ; specific heat of water at constant pressure
- $p_s = 101,325 \text{ kg m}^{-1} \text{ s}^{-2}$ ; surface pressure (also can be units Pascals).

Acknowledgements The authors wish to thank Hosmay Lopez, Dongmin Kim, and Stephanie Henderson for help with the LBM and Kelsey Malloy for help with the AGCM. We also thank the anonymous reviewers for their constructive feedback. The authors acknowledge the support from NOAA (NA18OAR4310293, NA15OAR4320064, NA20OAR4320472), NSF (OCE1419569, OCE1559151), and DOE (DE-SC0019433).

**Author contributions** MA (MA; corresponding author) wrote the main manuscript text and prepared all figures. MA and BK (BK; co-author) designed and executed modeling experiments and analyzed results. MA and BK reviewed the manuscript.

**Funding** The authors acknowledge the support from NOAA (NA18OAR4310293, NA15OAR4320064, NA20OAR4320472), NSF (OCE1419569, OCE1559151), and DOE (DE-SC0019433). BPK is the William R Middelthon Chair of Earth Sciences and is grateful for the associated support.

**Data availability** The NCEP-NCAR Reanalysis-2 data can be accessed online at https://psl.noaa.gov/data/gridded/data.ncep.Reanalysis2.html. The Rossby wave source term is calculated using the windspharm Python package (Dawson 2016).

### **Declarations**

Conflict of interest The authors declare that they have no conflict of interest.

Consent for publication The authors consent for publication.

**Ethics approval and consent to participate** The authors consent to participate and approve of all ethics guidelines.

### References

Alexander MA, Bladé I, Newman M, Lanzante JR, Lau N-C, Scott JD (2002) The atmospheric bridge: the influence of ENSO teleconnections on air–sea interaction over the global oceans. J Clim 15(16):2205–2231

Arcodia MC, Kirtman BP, Siqueira LS (2020) How MJO teleconnections and ENSO interference impacts us precipitation. J Clim 33(11):4621–4640

Becker EJ, Berbery EH, Higgins RW (2011) Modulation of cold-season us daily precipitation by the Madden–Julian oscillation. J Clim 24(19):5157–5166

Benedict JJ, Maloney ED, Sobel AH, Frierson DM, Donner LJ (2013) Tropical intraseasonal variability in version 3 of the GFDL atmosphere model. J Clim 26(2):426–449

Brenner S, Yang C-H, Mitchell K (1984) The AFGL global spectral model: expanded resolution baseline version. Technical report, Air Force Geophysics Lab Hanscom AFB MA

Cassou C (2008) Intraseasonal interaction between the Madden– Julian oscillation and the North Atlantic oscillation. Nature 455(7212):523

Collimore CC, Martin DW, Hitchman MH, Huesmann A, Waliser DE (2003) On the relationship between the QBO and tropical deep convection. J Clim 16(15):2552–2568

Dawson A (2016) Windspharm: a high-level library for global wind field computations using spherical harmonics. J Open Res Softw 4(1):1

Dawson A, Matthews AJ, Stevens DP (2011) Rossby wave dynamics of the north pacific extra-tropical response to El Niño: importance of the basic state in coupled GCMS. Clim Dyn 37(1):391–405

Densmore CR, Sanabia ER, Barrett BS (2019) QBO influence on MJO amplitude over the maritime continent: physical mechanisms and seasonality. Mon Weather Rev 147(1):389–406

Diaz HF, Hoerling MP, Eischeid JK (2001) Enso variability, teleconnections and climate change. Int J Climatol 21(15):1845–1862

Feng P-N, Lin H (2019) Modulation of the MJO-related teleconnections by the QBO. J Geophys Res Atmos 124(22):12022–12033



- Feng J, Liu P, Chen W, Wang X (2015) Contrasting Madden–Julian oscillation activity during various stages of EP and CP El Niños. Atmos Sci Lett 16(1):32–37
- Held IM, Lyons SW, Nigam S (1989) Transients and the extratropical response to El Nino. J Atmos Sci 46(1):163–174
- Henderson SA, Maloney ED (2018) The impact of the Madden– Julian oscillation on high-latitude winter blocking during El Niño-southern oscillation events. J Clim 31(13):5293–5318
- Henderson SA, Maloney ED, Barnes EA (2016) The influence of the Madden–Julian oscillation on northern hemisphere winter blocking. J Clim 29(12):4597–4616
- Henderson SA, Maloney ED, Son S-W (2017) Madden-Julian oscillation pacific teleconnections: the impact of the basic state and MJO representation in general circulation models. J Clim 30(12):4567–4587
- Hendon HH, Abhik S (2018) Differences in vertical structure of the Madden–Julian oscillation associated with the quasi-biennial oscillation. Geophys Res Lett 45(9):4419–4428
- Higgins R, Schubert S (1996) Simulations of persistent north pacific circulation anomalies and interhemispheric teleconnections. J Atmos Sci 53(1):188–207
- Hirota N, Takahashi M (2012) A tripolar pattern as an internal mode of the East Asian summer monsoon. Clim Dyn 39(9–10):2219–2238
- Hoell A, Barlow M, Wheeler MC, Funk C (2014) Disruptions of El Niño-southern oscillation teleconnections by the Madden– Julian oscillation. Geophys Res Lett 41(3):998–1004
- Hoskins BJ, Karoly DJ (1981) The steady linear response of a spherical atmosphere to thermal and orographic forcing. J Atmos Sci 38(6):1179–1196
- Hsu P-C, Fu Z, Xiao T (2018) Energetic processes regulating the strength of MJO circulation over the maritime continent during two types of El Niño. Atmos Ocean Sci Lett 11(2):112–119
- Kalnay E et al (1996) The NCEP/NCAR 40-year reanalysis project. Bull Am Meteorol Soc 77(3):437–472
- Kim B-M, Lim G-H, Kim K-Y (2006) A new look at the midlatitude-MJO teleconnection in the northern hemisphere winter. Q J R Meteorol Soc J Atmos Sci Appl Meteorol Phys Oceanogr 132(615):485–503
- Kim D, Lee S-K, Lopez H (2020) Madden–Julian oscillation-induced suppression of northeast pacific convection increases us tornadogenesis. J Clim 33(11):4927–4939
- Kirtman BP, Paolino DA, Kinter JL III, Straus DM (2001) Impact of tropical subseasonal SST variability on seasonal mean climate simulations. Mon Weather Rev 129(4):853–868
- Lappen C-L, Schumacher C (2012) Heating in the tropical atmosphere: What level of detail is critical for accurate MJO simulations in GCMS? Clim Dyn 39:2547–2568
- Lau K, Peng L (1987) Origin of low-frequency (intraseasonal) oscillations in the tropical atmosphere. Part I: basic theory. J Atmos Sci 44(6):950–972
- Lee RW, Woolnough SJ, Charlton-Perez AJ, Vitart F (2019) Enso modulation of MJO teleconnections to the North Atlantic and Europe. Geophys Res Lett 46(22):13535–13545
- Liess S, Geller MA (2012) On the relationship between QBO and distribution of tropical deep convection. J Geophys Res Atmos 117(D3):1
- Lim Y, Son S-W, Marshall AG, Hendon HH, Seo K-H (2019) Influence of the QBO on MJO prediction skill in the subseasonal-to-seasonal prediction models. Clim Dyn 53(3):1681–1695
- Lin H, Brunet G, Derome J (2007) Intraseasonal variability in a dry atmospheric model. J Atmos Sci 64(7):2422–2441
- Lin H, Brunet G, Derome J (2008) Forecast skill of the Madden– Julian oscillation in two Canadian atmospheric models. Mon Weather Rev 136(11):4130–4149

- Lin J, Mapes B, Zhang M, Newman M (2004) Stratiform precipitation, vertical heating profiles, and the Madden–Julian oscillation. J Atmos Sci 61(3):296–309
- Ling J, Zhao Y, Chen G (2019) Barrier effect on MJO propagation by the maritime continent in the MJO task force/gewex atmospheric system study models. J Clim 32(17):5529–5547
- Liu C, Tian B, Li K-F, Manney GL, Livesey NJ, Yung YL, Waliser DE (2014) Northern hemisphere mid-winter vortex-displacement and vortex-split stratospheric sudden warmings: influence of the Madden–Julian oscillation and quasi-biennial oscillation. J Geophys Res Atmos 119(22):12–599
- Liu J, Da Y, Li T, Hu F (2020) Impact of ENSO on MJO pattern evolution over the maritime continent. J Meteorol Res 34(6):1151–1166
- Lopez H, Dong S, Lee S-K, Campos E (2016) Remote influence of interdecadal pacific oscillation on the South Atlantic meridional overturning circulation variability. Geophys Res Lett 43(15):8250–8258
- Lopez H, Lee S-K, Dong S, Goni G, Kirtman B, Atlas R, Kumar A (2019) East Asian monsoon as a modulator of us great plains heat waves. J Geophys Res Atmos 1:1
- Malloy K, Kirtman BP (2022) The summer Asia–North America teleconnection and its modulation by ENSO in community atmosphere model, version 5 (CAM5). Clim Dyn 2022:1–18
- Mariotti A et al (2020) Windows of opportunity for skillful forecasts subseasonal to seasonal and beyond. Bull Am Meteorol Soc 101(5):E608–E625
- Matthews AJ, Hoskins BJ, Masutani M (2004) The global response to tropical heating in the Madden–Julian oscillation during the northern winter. Q J R Meteorol Soc J Atmos Sci Appl Meteorol Phys Oceanogr 130(601):1991–2011
- Mayer KJ, Barnes EA (2020) Subseasonal midlatitude prediction skill following quasi-biennial oscillation and Madden–Julian oscillation activity. Weather Clim Dyn 1(1):247–259
- Moon J-Y, Wang B, Ha K-J (2011) Enso regulation of MJO teleconnection. Clim Dyn 37(5–6):1133–1149
- Mori M, Watanabe M (2008) The growth and triggering mechanisms of the PNA: a MJO–PNA coherence. J Meteorol Soc Jpn Ser II 86(1):213–236
- Newman M, Sardeshmukh PD (1998) The impact of the annual cycle on the North Pacific/North American response to remote lowfrequency forcing. J Atmos Sci 55(8):1336–1353
- Nishimoto E, Yoden S (2017) Influence of the stratospheric quasi-biennial oscillation on the Madden–Julian oscillation during austral summer. J Atmos Sci 74(4):1105–1125
- Pang B, Chen Z, Wen Z, Lu R (2016) Impacts of two types of El Niño on the MJO during boreal winter. Adv Atmos Sci 33(8):979–986
- Pohl B, Matthews AJ (2007) Observed changes in the lifetime and amplitude of the Madden–Julian oscillation associated with interannual ENSO sea surface temperature anomalies. J Clim 20(11):2659–2674
- Riddle EE, Stoner MB, Johnson NC, L'Heureux ML, Collins DC, Feldstein SB (2013) The impact of the MJO on clusters of wintertime circulation anomalies over the North American region. Clim Dyn 40(7–8):1749–1766
- Riehl H (1950) On the role of the tropics in the general circulation of the atmosphere. Tellus 2(1):1–17
- Roundy PE, MacRitchie K, Asuma J, Melino T (2010) Modulation of the global atmospheric circulation by combined activity in the Madden–Julian oscillation and the El Niño-southern oscillation during boreal winter. J Clim 23(15):4045–4059
- Sardeshmukh PD, Hoskins BJ (1988) The generation of global rotational flow by steady idealized tropical divergence. J Atmos Sci 45(7):1228–1251
- Schumacher C, Houze RA Jr, Kraucunas I (2004) The tropical dynamical response to latent heating estimates derived from the TRMM precipitation radar. J Atmos Sci 61(12):1341–1358



- Seo K-H, Lee H-J (2017) Mechanisms for a PNA-like teleconnection pattern in response to the MJO. J Atmos Sci 74(6):1767–1781
- Seo K-H, Lee H-J, Frierson DM (2016) Unraveling the teleconnection mechanisms that induce wintertime temperature anomalies over the northern hemisphere continents in response to the MJO. J Atmos Sci 73(9):3557–3571
- Simmons A, Wallace J, Branstator G (1983) Barotropic wave propagation and instability, and atmospheric teleconnection patterns. J Atmos Sci 40(6):1363–1392
- Simpson J, Kummerow C, Tao W-K, Adler RF (1996) On the tropical rainfall measuring mission (TRMM). Meteorol Atmos Phys 60(1):19–36
- Son S-W, Lim Y, Yoo C, Hendon HH, Kim J (2017) Stratospheric control of the Madden–Julian oscillation. J Clim 30(6):1909–1922
- Stan C, Straus DM, Frederiksen JS, Lin H, Maloney ED, Schumacher C (2017) Review of tropical–extratropical teleconnections on intraseasonal time scales. Rev Geophys 55(4):902–937
- Stephens G, Smalley M, Lebsock M (2019) The cloudy nature of tropical rains. J Geophys Res Atmos 124(1):171–188
- Straus DM, Shukla J (2000) Distinguishing between the SST-forced variability and internal variability in mid latitudes: analysis of observations and GCM simulations. Q J R Meteorol Soc 126(567):2323–2350
- Straus DM, Swenson E, Lappen C-L (2015) The MJO cycle forcing of the North Atlantic circulation: intervention experiments with the community earth system model. J Atmos Sci 72(2):660–681
- Ting M, Sardeshmukh PD (1993) Factors determining the extratropical response to equatorial diabatic heating anomalies. J Atmos Sci 50(6):907–918
- Tseng K-C, Maloney E, Barnes E (2019) The consistency of MJO teleconnection patterns: an explanation using linear Rossby wave theory. J Clim 32(2):531–548
- Tseng K-C, Maloney E, Barnes EA (2020) The consistency of MJO teleconnection patterns on interannual time scales. J Clim 33(9):3471–3486
- Wang L, Li T, Chen L, Behera SK, Nasuno T (2018) Modulation of the MJO intensity over the equatorial western pacific by two types of El Niño. Clim Dyn 51(1):687–700

- Wang J, Kim H, Kim D, Henderson SA, Stan C, Maloney ED (2020a) MJO teleconnections over the PNA region in climate models. Part I: performance-and process-based skill metrics. J Clim 33(3):1051–1067
- Wang J, Kim H, Kim D, Henderson SA, Stan C, Maloney ED (2020b) MJO teleconnections over the PNA region in climate models. Part II: Impacts of the MJO and basic state. J Clim 33(12):5081–5101
- Watanabe M, Kimoto M (2000) Atmosphere—ocean thermal coupling in the North Atlantic: a positive feedback. Q J R Meteorol Soc 126(570):3343–3369
- Weare BC (2013) El Niño teleconnections in CMIP5 models. Clim Dvn 41(7):2165–2177
- Wei Y, Ren H-L (2019) Modulation of ENSO on fast and slow MJO modes during boreal winter. J Clim 32(21):7483–7506
- Wheeler MC, Hendon HH (2004) An all-season real-time multivariate MJO index: development of an index for monitoring and prediction. Mon Weather Rev 132(8):1917–1932
- Yadav P, Straus DM (2017) Circulation response to fast and slow MJO episodes. Mon Weather Rev 145(5):1577–1596
- Yeh S-W et al (2018) Enso atmospheric teleconnections and their response to greenhouse gas forcing. Rev Geophys 56(1):185–206
- Yoo C, Son S-W (2016) Modulation of the boreal wintertime Madden– Julian oscillation by the stratospheric quasi-biennial oscillation. Geophys Res Lett 43(3):1392–1398
- Zhang C (2005) Madden-Julian oscillation. Rev Geophys 43(2):1
- Zhang GJ, Mu M (2005) Simulation of the Madden–Julian oscillation in the NCAR CCM3 using a revised Zhang–Mcfarlane convection parameterization scheme. J Clim 18(19):4046–4064

**Publisher's Note** Springer Nature remains neutral with regard to jurisdictional claims in published maps and institutional affiliations.

Springer Nature or its licensor (e.g. a society or other partner) holds exclusive rights to this article under a publishing agreement with the author(s) or other rightsholder(s); author self-archiving of the accepted manuscript version of this article is solely governed by the terms of such publishing agreement and applicable law.

